How reliable are CMIP5 models in simulating dust optical depth?

Bing Pu[1,2] and Paul Ginoux[2]

[1]Atmospheric and Oceanic Sciences Program, Princeton University,

Princeton, New Jersey 08544

[2]NOAA Geophysical Fluid Dynamics Laboratory, Princeton, New Jersey 08540

Correspondence to: Bing Pu (bpu@princeton.edu)

1 **Abstract.** Dust aerosol plays an important role in the climate system by affecting the

2 radiative and energy balances. Biases in dust modeling may result in biases in simulating

3 global energy budget and regional climate. It is thus very important to understand how

4 well dust is simulated in the Coupled Model Intercomparison Project Phase 5 (CMIP5)

5 models. Here seven CMIP5 models using interactive dust emission schemes are

6 examined against satellite derived dust optical depth (DOD) during 2004-2016.

7   It is found that multi-model mean can largely capture the global spatial pattern

8 and zonal mean of DOD over land in present-day climatology in MAM and JJA. Global

9 mean land DOD is underestimated by -25.2% in MAM to -6.4% in DJF. While seasonal

10 cycle, magnitude, and spatial pattern are generally captured by multi-model mean over

11 major dust source regions such as North Africa and the Middle East, these variables are

12 not so well represented by most of the models in South Africa and Australia. Interannual

13 variations of DOD are neither captured by most of the models nor by multi-model mean.

14 Models also do not capture the observed connections between DOD and local controlling

15 factors such as surface wind speed, bareness, and precipitation. The constraints from

16 surface bareness are largely underestimated while the influences of surface wind and

17 precipitation are overestimated.

18   Projections of DOD change in the late half of the 21st century under the

19 Representative Concentration Pathways 8.5 scenario by multi-model mean is compared

20 with those projected by a regression model. Despite the uncertainties associated with both

21 projections, results show some similarities between the two, e.g., DOD pattern over

22 North Africa in DJF and JJA, an increase of DOD in the central Arabian Peninsula in all

23 seasons, and a decrease over northern China from MAM to SON.

1. Introduction

Dust is the second most abundant aerosols by mass in the atmosphere after sea salt. It absorbs and scatters both shortwave and longwave radiation and thus modifies local radiative budget and consequently vertical temperature profile, influencing global and regional climate. For instance, studies found dust influences the strength of the West African monsoon (e.g., Miller and Tegen, 1998; Miller et al., 2004; Mahowald et al., 2010; Strong et al., 2015) and Indian monsoonal rainfall (e.g., Vinoj et al., 2014; Jin et al., 2014, 2015, 2016; Solmon et al., 2015; Kim et al., 2016; Sharma and Miller, 2017). Dust aerosols are also found to amplify droughts during the U.S. Dust Bowl and Medieval Climate Anomaly (Cook et al., 2008, 2009, 2013), and affect Atlantic tropical cyclones (e.g., Dunion and Velden, 2004; Wong and Dessler, 2005; Evan et al., 2006; Sun et al., 2008; Strong et al., 2018). Dust particles can also serve as ice cloud nuclei and influence the properties of the cloud (e.g., Levin et al., 1996; Rosenfield et al., 1997; Wurzler et al., 2000; Nakajima et al., 2001; Bangert et al., 2012) and affect regional radiative balance and hydrological cycle. When deposited in the oceans, iron-enriched dust also provides nutrients for phytoplankton, affecting ocean productivity and therefore carbon and nitrogen cycles and ocean albedo (e.g., Fung et al., 2000; Jickells et al., 2005; Shao et al., 2011).

Globally, the estimated radiative forcing from dust aerosol is 0.10 (-0.30 to +0.10) W m^{-2}, a magnitude about one fourth of the radiative forcing of sulfate aerosol or black carbon from fossil fuel and biofuel (Myhre et al., 2013; their Table 8.4). Biases in dust simulation may potentially affect global energy budgets and regional climate simulation.

46   Thus, it is very important to examine the capability of current state-of-the-art climate

47   models in simulating dust.

48   Only a few studies examined the Coupled Model Intercomparison Project Phase 5

49   (CMIP5) model output of dust and most of them are regional evaluations. For instance,

50   Evan et al. (2014) examined model output for Africa, but mainly focused on an area over

51   the northeastern Atlantic (10°–20°N and 20°–30°W) where a long-term proxy of dust

52   optical depth data over Cape Verde islands is available (Evan and Mukhopadhyay, 2010).

53   They found models underestimated dust emission and mass path and failed to capture the

54   interannual variations from 1960 to 2004, as models did not capture the negative

55   connection between dust mass path and precipitation over the Sahel.

56   Another work examined CMIP5 aerosol optical depth (AOD) is by Sanap et al.

57   (2014) for India. They compared dust distribution in the models with Earth Probe total

58   ozone monitoring system (EPTOMS)/ Ozone monitoring Instrument (OMI) aerosol index

59   (AI) from 2000 to 2005. They found most of CMIP5 models, except two HadGEM2

60   models, underestimated dust load over Indo-Gangetic Plains, and suggested the biases are

61   due to a misrepresentation of 850 hPa winds in the models. Later, Misra et al. (2016) also

62   examined CMIP5 modeled AOD for India but did not specifically focus on dust.

63   Shindell et al. (2013) examined the output of 10 models from the Atmospheric

64   Chemistry and Climate Model Intercomparison Project (ACCMIP) for one year (2000),

65   among which eight models also participated in the CMIP5. They noticed that simulated

66   dust AOD vary by more than a factor of two across models. However, this study also did

67   not focus on dust, but emphasized the radiative forcings from anthropogenic aerosols.

68   None of the above studies examined global dust simulation in CMIP5 models.

69   What's more, most studies focused on annual mean, not seasonal averages. It is very

70   possible that models perform better in some seasons than others. AeroCom multiple-dust

71   model intercomparison was performed on both global and regional scales (Huneeus et al.,

72   2011) but only focused on one year, thus models' capability of simulating interannual or

73   long-term variability of dust is not clear. A comprehensive evaluation of the climatology

74   and interannual variation of global dust optical depth (DOD) in CMIP5 models will

75   provide insights into models' capability of simulating the integrated aerosol extinction

76   due to dust, which is one of the key variables that determine the radative forcing of dust

77   to the climate system.

78   Here we examine the results of seven CMIP5 models (Table 1) by comparing

79   model output with DOD derived from Moderate Resolution Imaging Spectroradiometer

80   (MODIS) Deep Blue aerosol products. Projections on changes of DOD in the late half of

81   the 21st century by CMIP5 models and also by a regression model (Pu and Ginoux, 2017)

82   are examined and analyzed. The following section introduces data and methods used in

83   this study. Results are presented in section 3, including examinations on the climatology

84   and interannual variations of CMIP5 DOD and future projections. Discussion and major

85   conclusions are presented in sections 4 and 5, respectively.

86

87   **2. Data and Methodology**

88   **2.1 DOD from MODIS**

89   DOD is a widely used variable that describes optical depth due to the extinction

90   by mineral particles. It is one of the key factors (single scattering albedo and asymmetry

91 factor being the two others) controlling dust interaction with radiation. Monthly DOD are

92 derived from MODIS aerosol products retrieved using the Deep Blue (MDB2) algorithm,

93 which employs radiance from the blue channels to detect aerosols globally over land even

94 over bright surfaces, such as desert (Hsu et al., 2004, 2006). Ginoux et al. (2012b) used

95 collection 5.1 level 2 aerosol products from MODIS aboard the Aqua satellite to derive

96 DOD. Here, both MODIS aerosol products (collection 6, level 2; Hsu et al., 2013) from

97 the Aqua and Terra platforms are used. Aerosol products such as AOD (550 nm), single

98 scattering albedo, and the Ångström exponent are first interpolated to a regular 0.1° by

99 0.1° grid using the algorithm described by Ginoux et al. (2010). The DOD is then derived

100 from AOD following the methods of Ginoux et al. (2012b) with adaptions for the newly

101 released MODIS collection 6 aerosol products (Pu and Ginoux, 2016). To separate dust

102 from other aerosols, we use the Ångström exponent (α) and single scattering albedo (ω).

103 Ångström exponent has been shown to be highly sensitive to particle size (Eck et al.,

104 1999). A continuous function relating the Ångström exponent to fine-mode aerosol

105 optical depth established by Anderson et al. (2005; their Eq. 5) based on ground-based

106 data is used to separate dust from fine particles. We also screen the data by setting single

107 scattering albedo at 470 nm to be less than one for dust due to its absorption of solar

108 radiation. This separates dust from scattering aerosols such as sea salt, which is purely

109 scattering. The formula can be summarized as the following:

110 $$DOD = AOD \times (0.98\text{-}0.5089\alpha + 0.0512\alpha^2) \quad \text{if} (\omega < 1) \qquad . \qquad (1)$$
111

112 Note that DOD represents the coarse mode fraction of dust only. It is estimated that the

113 fine mode dust at emission is less than 10% (Kok et al., 2017).

114   Aqua and Terra DOD have previously been used to study global dust sources

115   (Ginoux et al., 2012b), and their geomorphological signature (Baddock et al., 2016), dust

116   variations in the Middle East (Pu and Ginoux, 2016) and the U.S. (Pu and Ginoux, 2017),

117   and have been validated with Aerosol Robotic NETwork (AERONET) stations over the

118   U.S. (Pu and Ginoux, 2017). Here we compare Aqua and Terra DOD against AERONET

119   stations globally (Section 1 and Figures. S1-2 in the Supplement). Both Aqua and Terra

120   DOD is slightly underestimated, with respective errors of 0.08+0.52DOD and

121   0.10+0.48DOD.

122   Daily DOD from Aqua and Terra are averaged to monthly data and interpolated to

123   a 1° by 1° grid. Terra passes the Equator from north to south around 10:30 local time

124   while Aqua passes the Equator from south to north around 13:30 local time. To reduce

125   missing data and also to combine the information from both morning and afternoon

126   hours, a combined monthly DOD (here after MODIS DOD) is derived by averaging Aqua

127   and Terra DOD when both products exist or using either Aqua or Terra DOD when only

128   one product is available. As shown in Figure S3 in the Supplement, the mean available

129   days in each season and also spatial coverage are enhanced in combined DOD than using

130   Aqua or Terra (not shown) DOD alone. This combined DOD is available from January

131   2003 to December 2016.

132   We also compared MODIS DOD climatology with both AERONET observation

133   and DOD retrieved from Cloud-Aerosol Lidar with Orthogonal Polarization (CALIOP;

134   Winker et al., 2004; 2007) aboard the Cloud-Aerosol Lidar and Infrared Pathfinder

135   Satellite Observation (CALIPSO) satellite. AERONET stations provide cloud-screened

136   and quality assured (level 2) coarse mode aerosol optical depth (COD) at 500 nm, which

137   is processed by the Spectral Deconvolution Algorithm (O'Neill et al., 2003). Only nine

138   sites have long-term COD records during 2003-2016, and the climatological mean of

139   MODIS DOD generally compares well with these sites (Figure S4 in the Supplement).

140   CALIOP measures backscattered radiances attenuated by the presence of aerosols

141   and clouds and retrieves corresponding microphysical and optical properties of aerosols.

142   Monthly dust AOD (or DOD) on a 2° latitude by 5° longitude grid are available since

143   June 2006. The climatology of CALIOP DOD during 2007-2016 is similar to that of

144   MODIS DOD during the same period (Figure S5 in the Supplement). The global mean

145   (over land) MODIS DOD is slightly higher than that from CALIOP, probably due to the

146   lower horizontal resolution of the latter. The pattern correlations (e.g., Pu et al., 2016)

147   between the two products range from 0.83 in boreal spring and summer to 0.63 in boreal

148   winter (Figure S5 in the Supplement). Due to higher spatial resolution (compared with

149   CALIOP) and coverage (compared with AERONET sites), MODIS DOD is chosen as the

150   primary product to validate CMIP5 model output. Nine regions (Table 2) are selected to

151   study the DOD magnitude, spatial pattern, and variations. These regions cover major dust

152   source regions previously identified (Ginoux et al. 2012).

153   Given the analysis above (Figs. S3-5), there are some uncertainties associated

154   with DOD in a few regions in some seasons: (1) relatively low coverage (<30 days per

155   season) over northern China and southeastern Asia in JJA; (2) DOD is slightly higher

156   than COD from AERONET over the Arabian Peninsula in DJF and SON; (3) DOD is

157   lower than CALIOP over northern India in MAM. We will consider these uncertainties in

158   the following analysis wherever is relevant.

159

2.2 Reanalysis and observation datasets

160

161 Previous study found that the variations of dust event frequency over the U.S. in

162 the recent decade could be largely represented by the variations of three local controlling

163 factors: seasonal mean surface wind speed, bareness, and precipitation (Pu and Ginoux,

164 2017). These factors have previously been found to constrain dust emission or variability

165 on multiple time scales (e.g., Gillette and Passi, 1988; Fecan et al., 1999; Zender and

166 Kwon, 2005). While surface wind is positively related to the emission and transport of

167 dust, vegetation is an important non-erodible element that prevents wind erosion.

168 Precipitation is generally negatively related to dust emission and transport processes.

169 While the scavenging effect of precipitation on small dust particles only lasts a few hours

170 or days, influences of precipitation on soil moisture lasts longer.

171 To examine the interannual variations of DOD and its connection with local

172 controlling factors such as surface wind speed, bareness, and precipitation, monthly data

173 of 10 m wind speed from the ERA-Interim (Dee et al., 2011), leaf area index (LAI) data

174 from Advanced Very High Resolution Radiometer (AVHRR; Claverie et al., 2014,

175 2016), and precipitation from the Precipitation Reconstruction over Land (PRECL; Chen

176 et al., 2002) are used.

177 ERA-Interim is a global reanalysis from the European Centre for Medium-Range

178 Weather Forecasts (ECMWF). Its horizontal resolution is T255 (about 0.75° or 80 km).

179 We choose this analysis because of its relatively high spatial resolution. The monthly data

180 are available from 1979 to present day.

181 Monthly LAI derived from the version 4 of Climate Data Record (CDR) of

182 AVHRR is used to calculate surface bareness. The data are produced by the National

183   Aeronautics and Space Administration (NASA) Goddard Space Flight Center (GSFC)

184   and the University of Maryland. Monthly gridded data on a horizontal resolution of 0.05°

185   by 0.05° degree are available from 1981 to present. This product is selected due to its

186   high spatial resolution and long temporal coverage. Surface bareness is calculated from

187   seasonal mean LAI (Pu and Ginoux, 2017) as the following,

188   *Bareness = exp (-LAI)*   .   (2)

189   Bareness is originally defined as *exp (-LAI-SAI)*, where *SAI* is stem area index (Evans et

190   al. 2016). Since satellite does not retrieve brownish SAI, we only use LAI to calculate

191   bareness.

192   PRECL precipitation from the National Oceanic and Atmospheric Administration

193   (NOAA) is a global analysis available monthly from 1948 to present at a 1° by 1°

194   resolution. The dataset is derived from gauge observations from the Global Historical

195   Climatology Network (GHCN), version 2, and the Climate Anomaly Monitoring System

196   (CAMS) datasets. Its long coverage and spatial resolution is suitable to study the

197   connections between DOD and precipitation.

198

199   **2.3 CMIP5 model output**

200   Among CMIP5 models we selected seven models (Table 1) that used interactive

201   dust emission schemes, in which dust emission varied in response to changes of climate.

202   The output of 10 m wind speed, precipitation, and LAI are also available from these

203   models. In models that dust is simulated offline, i.e., dust emission did not interactively

204   respond to meteorological and climate changes, the connections between DOD and

205   modeled controlling factors are lost. Other models (to our best knowledge) either used

206 offline dust as an input or did not write out the variables needed for this analysis.

207   Both historical run from 1861 to 2005 and future run under the Representative

208 Concentration Pathways 8.5 (RCP 8.5) scenario (Riahi et al., 2011) from 2006 to 2100

209 are used. Here the RCP 8.5 scenario is chosen because it represents the upper limit of the

210 projected greenhouse gas change in the twenty-first century and thus likely is the worst-

211 case scenario for future DOD variation under climate change. Also, studies found that

212 observed CO_2 emission pathway during 2005-2014 matches RCP 8.5 scenario better than

213 other scenarios (e.g., Fuss et al., 2014), which makes the RCP8.5 output suitable to

214 examine present-day DOD variations after 2005.

215   Monthly model output of dust load, surface 10 m wind speed, precipitation, and

216 LAI are used. Historical output from 2003 to 2005 and RCP 8.5 output from 2006 to

217 2016 are combined to form time series and climatology during 2003-2016 to compare

218 with MODIS DOD during the same time period.

219

220 **2.3.1 DOD derived from modeled dust load**

221   Most CMIP5 models did not save DOD, so we used monthly dust load and

222 converted them to DOD using the relationship derived by Ginoux et al. (2012a) as the

223 following

224 $$\tau = M \times e \ ,$$ (3)

225 where τ is DOD at 500 nm, M is the load of dust in unit of (g m^{-2}), and $e = 0.6$ m^2 g^{-1} is

226 the mass extinction efficiency. Dust load from different models is first interpolated to a

227 2° by 2.5° grid and then converted to DOD. The same method was used by Pu and

228 Ginoux (2017) for the U.S. Applying the same mass extinction efficiency everywhere

229 and to all the CMIP5 model output used here is a simplification, as different models may

230 have quite different mass extinction efficiency. For instance, e can range from 0.25 to

231 1.28 m^2 g^{-1} in AEROCOM models, with a multi-model medium of 0.72 m^2 g^{-1} (Huneeus

232 et al., 2011). Here, we compare the derived DOD with modeled DOD from one historical

233 simulation of GFDL-CM3 model (Donner et al., 2011) as an example. A full validation

234 of this method will require modeled DOD from all the other CMIP5 models, which are

235 currently not available. The pattern correlation of the climatology (1861-2005) between

236 the derived DOD and modeled DOD in GFDL-CM3 are very high, all above 0.99 for four

237 seasons (not shown). The percentage differences between derived DOD and modeled

238 DOD averaged over global land range from -3.6% in DJF and SON to 1.3% in MAM and

239 JJA.

240

241 **2.4 A linear regression model**

242 **2.4.1 Multiple linear regression**

243 In order to examine the relative contribution of each local controlling factor to

244 DOD variations, multiple linear regression is applied by regressing MODIS DOD onto

245 standardized seasonal mean ERA-Interim surface wind speed, AVHRR bareness, and

246 PRECL precipitation at each grid point. All the data are re-gridded to a 1° by 1° grid

247 before the calculation. Over regions where values are missing for any of the explanatory

248 variables (i.e., precipitation, bareness, and surface wind speed) or DOD, the regression

249 coefficients are set to missing values. The collinearity among these explanatory variables

250 is examined by calculating variance inflation factor (VIF) (e.g., O'Brien, 2007; Abudu et

251 al., 2011), and in most regions the VIF is below 2 (not shown), indicating a low

252 collinearity (5–10 is usually considered high). Bootstrap resampling is used to test the

253 significance of the regression coefficients, following the method used by Pu and Ginoux

254 (2017).

255   Multiple linear regression is also applied to CMIP5 model derived DOD and

256 output of surface wind speed, bareness, and precipitation to obtain regression coefficients

257 from the models from 2004 to 2016. All variables are interpolated to a 2° by 2.5° grid

258 before regression. The results are compared with regression coefficients derived from

259 observational datasets.

260

261 **2.4.2 DOD reconstruction and future projection**

262   Using regression coefficients obtained from observations and observed variations

263 of precipitation, bareness, and surface wind speed from 2004 to 2016, we can reconstruct

264 DOD in the present day and compare it with MODIS DOD (see discussion in section 3.2).

265   Similar to the method used by Pu and Ginoux (2017), the regression coefficients

266 derived from MODIS DOD and observed controlling factors and CMIP5 model output of

267 surface wind speed, bareness, and precipitation are used to project variations of future

268 DOD. The regression coefficients are interpolated from the 1° by 1° grid to a 2° by 2.5°

269 grid to be consistent with model output. Such an interpolation may smooth out some

270 spatial characteristics from observations. Here we tried two groups of CMIP5 output for

271 these controlling factors. One group used seven models with interactive dust emission

272 scheme (Table 1), and the other used 16 CMIP5 models (see Supplementary Table S1 of

273 Pu and Ginoux, 2017) that include the seven models with interactive dust emission

274 scheme. The reason to test the latter is to include as much model output of the controlling

275 factors as possible. The differences between the historical run (1861–2005 average) and

276 that of the RCP 8.5 run for the late half of the twenty-first century (2051–2100) are

277 standardized by the standard deviation of the historical run for each explanatory variable.

278 The projected change reveals how DOD will vary with reference to the historical

279 conditions (mean and standard deviation).

280

281 **3. Results**

282 **3.1 Climatology (2004-2016)**

283 Figure 1 shows the climatology of MODIS DOD (top panel) in four seasons

284 during 2004-2016 and that from the CMIP5 multi-model mean (bottom). Globally, the

285 dustiest regions are largely located over the northern hemisphere (NH) over North Africa,

286 the Middle East, and East Asia (Figs. 1a-d). In these regions, DOD is higher in boreal

287 spring and summer than fall and winter. Modeled global DOD over land is generally

288 lower than that from MODIS DOD, ranging from -0.028 (-25.2%) in MAM to -0.005 (-

289 6.4%) in DJF. The global spatial pattern is better captured in MAM and JJA, with pattern

290 correlations of 0.74 and 0.85, respectively (Figs. 1f-g). In DJF, DOD is overestimated

291 over central Africa and Australia, but underestimated over the Middle East and Asia (Fig.

292 1e), while in SON there is a similar overestimation in Australia and an underestimation in

293 the Middle East (Fig. 1h).

294 Figure 2 shows the zonal mean of CMIP5 DOD from individual models (thin

295 colorful lines) and multi-model ensemble mean (thick black), in comparison with MODIS

296 DOD (thick red). In DJF, DOD is underestimated in the NH from 15° N to 50°N but

297 overestimated over the tropics and southern hemisphere (SH) (Fig. 2a). While the

298   overestimation in the SH is largely contributed by three models, the underestimation in

299   the NH appears in all the seven models. The overestimation of DOD in HadGEM2-ES

300   has also been identified in a previous study (Bellouin et al., 2011) and will be discussed

301   later. In MAM, a similar overestimation of DOD in the tropics and SH also occurs in

302   some models, and the multi-model mean slightly overestimates DOD around 20°-30°S

303   (Fig. 2b). In NH, there is a weak underestimation too, but the overall gradient is largely

304   captured. In JJA, the multi-model mean resembles MODIS DOD very well (Fig. 2c),

305   consistent with the highest pattern correlation in this season shown in Fig. 1. The peak

306   around 19° N in North Africa and Middle East is well captured by the multi-model mean,

307   although the magnitude is slightly underestimated. In SON, different from MODIS DOD

308   that peaks around 19°N, the multi-model mean has two peaks around 15°N and 28°S,

309   respectively, a pattern somewhat similar to that in DJF (Fig. 2d). Consequently, DOD in

310   CMIP5 multi-model mean is overestimated at 15°-40°S and 0°-15°N but underestimated

311   at 15°S -0° and 15°-40°N.

312   Seasonal cycles of CMIP5 DOD are compared with MODIS DOD in nine regions

313   in Figure 3. The annual means of DOD in each region from multi-model mean (black)

314   and MODIS (red) are also listed in each plot. The spread of DOD among individual

315   models is greater during boreal spring and summer for regions in the NH and during

316   austral spring and summer for regions in the SH. Seasonal cycles over North Africa, the

317   Middle East, North America, and India are generally captured by multi-model mean, with

318   modeled DOD peaking during the same seasons as MODIS DOD (Figs. 3a-b, d-e). While

319   some models overestimate the seasonal peaks over the Middle East, North America, and

320   India (e.g., CanESM2, HadGEM2-ES, and HadGEM2-CC), a few models have very

321   weak seasonal cycles and underestimate DOD over North America and India (e.g.,

322   GFDL-CM3, NorESM1-M, MIROC-ESM, and MIROC-ESM-CHEM). Note that

323   MODIS DOD is slightly lower than CALIOP DOD over India in MAM (Fig. S5),

324   therefore for these models the underestimation may be larger than shown in Fig. 3e.

325   Since the temporal coverage of MODIS DOD over northern China and

326   southeastern Asia is relatively low in JJA compared with other regions (Fig. S3), we also

327   examined the seasonal cycle of CALIOP DOD (not shown) and results are similar but

328   with weaker magnitude. Over northern China, MODIS DOD peaks in spring (Fig. 3c),

329   consistent with previous studies (e.g., Zhao et al., 2006; Laurent et al., 2006; Ginoux et

330   al., 2012b), while multi-model mean peaks later in May-June. Individual models have

331   quite different seasonal cycles, with GFDL-CM3 model having a peak (in April) closer to

332   the timing of MODIS maximum. Similar misrepresentation occurs over the southeastern

333   Asia (Fig. 3f).

334   In South Africa and South America the observed maxima in early austral spring

335   (i.e., September) are also not captured by the multi-model mean (Figs. 3g-h). Note that

336   CanESM2 largely captures the seasonal cycle of DOD over South America, although the

337   magnitude is overestimated (Fig. 3h). In Australia, DOD is largely overestimated and the

338   peak from November to January in MODIS DOD is shifted about one month earlier in

339   the multi-model mean (Fig. 3i). Similar to the finding here, Bellouin et al. (2011) also

340   found that HadGEM2-ES model overestimated DOD over Australia and Thar desert

341   region in northwestern India and suggested that these overestimations were likely due to

342   model's overestimation of bare soil fraction and underestimation of soil moisture. Despite

343   overestimation, the seasonal cycle in HadGEM2-CC model is more similar to MODIS

344   DOD than other models (Fig. 3i).

345   We further examine the magnitudes and spatial patterns of CMIP5 DOD in these

346   regions. Figure 4 shows the ratio of pattern standard deviations (standard deviations of

347   values within the domain) and pattern correlation between CMIP5 DOD and MODIS

348   DOD climatology (2004-2016) in each region for four seasons. While the former reveals

349   the magnitude differences, the latter demonstrates the spatial resemblance.

350   Over North Africa, the Middle East, and India, the ratio of CMIP5 DOD from

351   individual models and multi-model mean versus MODIS DOD are all within ± one order

352   of magnitude (Fig. 4). Most models underestimate DOD in northern China, although the

353   magnitudes are largely within the range of -one order of magnitude to one. Over North

354   America, South Africa, and Australia, some models underestimate the DOD by more than

355   two orders of magnitudes, while over Australia three models overestimate DOD by more

356   than one order of magnitude. In general, magnitudes of multi-model mean are closer to

357   satellite DOD than most individual models and are largely within ± one order of

358   magnitude of MODIS DOD.

359   The spatial patterns are better captured over North Africa and the Middle East

360   than other regions (Fig. 4), with pattern correlations above 0.6 in most models (with

361   highest pattern correlation of 0.92 and 0.83, respectively). Pattern correlations from

362   multi-model mean are also high, reaching 0.87 (0.78) over North Africa and 0.75 (0.73)

363   over the Middle East in JJA (MAM). Nonetheless, some models show negative pattern

364   correlations over North Africa, northern China, North America, southeastern Asia, South

365   Africa, South America, and Australia. Overall, spatial patterns are less well represented

366   in regions over the SH than over the NH in CMIP5 models.

367   In short, in terms of both magnitudes and spatial pattern, DOD climatology is best

368   represented over North Africa and the Middle East among the nine regions. The multi-

369   model mean shows that DOD over North Africa is slightly better simulated than over the

370   Middle East, somewhat similar to the finding of AeroCom multi-model analysis

371   (Huneeus et al. 2011).

372

373   **3.2 Interannual variations**

374   An important aspect of dust activity is its long-term variability, including

375   interannual and decadal variations. Dust emission in North Africa is known to have

376   strong decadal variations (e.g., Prospero and Nees, 1986; Prospero and Lamb, 2003;

377   Mahowald et al., 2010; Evan et al., 2014, 2016), while over Australia, strong interannual

378   variations have been related to El Niño–Southern Oscillation (e.g., Marx et al., 2009;

379   Evans et al., 2016). Due to the short time coverage of high quality satellite products, we

380   focus on interannual variations of DOD from 2004 to 2016.

381   Figure 5 shows the correlations of regional mean time series of DOD between

382   MODIS and CMIP5 models and multi-model mean for each season in nine regions. We

383   also show correlations between the reconstructed DOD (see section 2.4.2 for details) and

384   MODIS DOD for reference (Table S1 in the Supplement). The reconstructed DOD is

385   calculated using observed regression coefficients and time-varying controlling factors

386   from observations (i.e., surface wind speed, bareness, and precipitation).

387   The interannual variations of DOD are in general not well captured by CMIP5

388   models. This is consistent with previous study by Evan et al. (2014) who found dust

389   variability downwind of North Africa over the northeastern Atlantic was misrepresented

390   in CMIP5 models. In most regions, only one or two models show significant positive

391   correlation with MODIS DOD in some seasons, and negative correlations exist in all

392   regions (Fig. 5). North Africa, the Middle East, southeastern Asia, South America, and

393   Australia show less negative correlations than other dusty regions. On the other hand,

394   reconstructed DOD shows significant positive correlations with MODIS DOD over most

395   regions in all seasons (Table S1 in the Supplement). This suggests that the interannual

396   variations of DOD can be largely attributed to the variations of these controlling factors,

397   and models may misrepresent these relationships, in addition to their incapacity of

398   capturing the interannual variations of individual controlling factors in general (not

399   shown), which is not uncommon for coupled models.

400   We further examine the connection between those controlling factors and DOD in

401   CMIP5 models. Figure 6 shows the dominant controlling factors among the three (surface

402   wind speed, bareness, and precipitation) on DOD variations in four seasons from MODIS

403   (left column) and from CMIP5 multi-model mean (right column), respectively. To

404   highlight factors controlling DOD variations near the dust source regions, a mask of

405   AVHRR LAI≤ 0.5 is applied to both coefficients.

406   Bareness plays the most important role in many dusty regions in observations,

407   e.g., over Australia, central U.S., and South America (Figs. 6a-d). Note that while

408   bareness plays an important role over the Sahel during DJF and MAM, it also shows

409   strong signal over some areas in the northern North Africa (Figs. 6a-b). The reliability of

410   this information is limited by the accuracy of LAI retrieval in these areas. The value of

411   bareness in this region is actually quite high (as LAI is very low), but still has weak

412   interannual variability (Figures S6 in the Supplement). Over some areas of North and

413   South Africa, the Middle East, and East Asia, surface wind and precipitation are also

414   quite important.

415   The role of bareness is largely underestimated in CMIP5 models, while surface

416   wind and precipitation become the dominant factors (Figs. 6e-h). The misrepresentation

417   of the connection between DOD and these controlling factors may cause the

418   misrepresentation of the dust load and its variability. Taking Australia for an example,

419   the overestimation of DOD magnitudes may be related to an overestimation of the

420   influence of surface wind on DOD and a lack of constraints from surface bareness.

421   Despite the large differences between the observed and modeled connections

422   between DOD and the controlling factors, some regions show similarities. For instance,

423   over North Africa in DJF, both show an important influence from surface winds (Figs.

424   6a, e), although the locations of surface wind-dominant areas are not exactly the same.

425   Evan et al. (2016) also found a dominant role of surface wind on African dust variability,

426   but they focused on monthly means, not seasonal averages. In MAM, precipitation starts

427   to play a role in some parts of North Africa, while surface wind still dominates in some

428   areas (Fig. 6b). Same increasing influence of precipitation is shown in the multi-model

429   mean, but such an influence seems overestimated (Fig. 6f). In JJA, the influences of

430   precipitation and bareness over the eastern Arabian Peninsula in the multi-model mean

431   (Fig. 6g) also show some similarity to observation (Fig. 6c), although an underestimation

432   of the influence from bareness and an overestimation of precipitation are still there.

433   Also, note that in CMIP5 models, due to lack of constraints from low surface

434   temperature (e.g., over frozen land) and snow cover on dust emission or

435   misrepresentations of dust transport, DOD and also the regression coefficients still exist

436   over NH high latitudes in boreal winter and spring in the multi-model mean (Figs. 6e-f).

437

438   **3.3 Future projections**

439   How will DOD change in response to increasing greenhouse gases? The results

440   from CMIP5 multi-model mean are shown in Figure 7. We compare the DOD during the

441   late half of the 21st century under the RCP 8.5 scenario with that in the historical level

442   (1861-2005 average).

443   Over land, CMIP5 model projects a decrease of global mean DOD in all seasons

444   except JJA (Figs. 7a-d). The inter-model standard deviation is much greater than the

445   multi-model mean, suggesting large discrepancies among individual models. The

446   projected decrease is largely over northern North America, southern North Africa, eastern

447   central Africa, and East Asia, while the increase is largely over northern North Africa, the

448   Middle East, southern North America, South Africa, South America, and southern

449   Australia (Fig. 7). Regional means of DOD change (in percentage) with reference to

450   CMIP5 historical run are summarized in Table 3.

451   What might be the causes of DOD change? Figure 8 shows the projected change

452   of precipitation, bareness, and surface wind speed from CMIP5 multi-model mean. These

453   factors play important role in DOD variations in the present day, although models tend to

454   underestimate the role of bareness and overestimate the influences of precipitation and

455   surface wind (Fig. 6). Increases in precipitation can increase soil moisture and remove

456   airborne dust, thus usually favors a decrease of DOD. As shown in Figs. 8a-d, the

457   increases of precipitation in northern Eurasia, northern North America, the Congo basin

458   in Africa, and Australia (DJF and MAM) may contribute to the decrease of DOD in these

459   regions, while the decreases of precipitation over northern North Africa and the Middle

460   East (DJF and MAM), South Africa, and South America may contribute to the increase of

461   DOD (DJF-SON). Also note that in JJA both precipitation and DOD increase over

462   northern North Africa and the Middle East (Fig. 8c), suggesting other factors dominate

463   the variation of DOD in the multi-model mean.

464   A decrease (increase) of bareness indicates a growth (decay) of vegetation and is

465   usually associated with a decrease (increase) of DOD. In general, except regions such as

466   southern North America, South America, South Africa, part of northern Eurasia, and

467   central Sahel, the pattern of bareness change does not resemble DOD change (Figs. 8e-h).

468   This is probably due to the fact that the overall influence of bareness on DOD variation is

469   underestimated in CMIP5 models (Fig. 6).

470   Increases in surface wind can enhance dust emission and transport, and vise versa.

471   The changes of surface wind in DJF and MAM are similar and likely to contribute to the

472   increase of DOD over northern North Africa, the Middle East, eastern South America,

473   southern South Africa, and southern Australia (Figs. 8i-j). The decrease of DOD over

474   northwestern North America, the Sahel, and northern Australia may also relate to the

475   decrease of surface wind there, in addition to an increase of precipitation and a reduction

476   of bareness. In JJA and SON (Figs. 8k-l), the increases of surface wind in South America,

477   South Africa, central Australia and the decreases of wind in northwestern North America,

478   northern Eurasia, and the central Sahel are also consistent with patterns of DOD change.

479   In short, variations of CMIP5 DOD in the late half of the 21st century are more

480   consistent with changes of precipitation and surface wind speed than with surface

481   bareness, consistent with the analysis above regarding to the present-day condition.

482   Here we also present the projected change of DOD from the regression model in

483   Figure 9. The regression model (see section 2.4 for details) is developed based on

484   observed relationships between MODIS DOD and local controlling factors and can

485   largely capture the interannual variations of DOD in the present-day climate (Table S1 in

486   the Supplement). Assuming that the observed connection between DOD and these

487   controlling factors do not change dramatically in the future, we can use this regression

488   model and CMIP5-model projected change of controlling factors to project DOD

489   variations. Compared to DOD projection from CMIP5 models, this approach utilizes

490   additionally observational constrains and is likely to provide a more reliable future

491   projection. We use projected changes of precipitation, bareness, and surface wind speed

492   from seven CMIP5 models with interactive dust emission scheme (see methodology). A

493   similar method is applied to the model output from 16 CMIP5 models, and results are

494   similar (Figure S7 in the Supplement). A mask of present-day LAI $\leq$ 0.5 is also applied to

495   highlight the changes of DOD near dust source regions. By doing this, we assume the

496   location of major dust sources will not change much at the late half of the 21st century.

497   The unmasked figure is presented in the supplementary file (Figure S8 in the

498   Supplement). The reason we did not use the projected future LAI as a mask is that

499   there're large uncertainties associated with LAI projection, especially over northern

500   hemisphere subtropical regions (e.g., Figs. 8e-h).

501   In DJF, regression model projected change of DOD over Mexico, North Africa,

502   the Middle East and part of northern China (Fig. 9a) are similar to those projected by

503   CMIP5 models over those dust source regions (Fig. 7a), but with a greater magnitude. In

504   MAM, a decrease of DOD is projected over large area of North Africa (Fig. 9b), which is

505   different from the pattern projected from the CMIP5 multi-model mean (Fig. 7b). The

506   decrease of DOD over northern central U.S. is also different from the overall increase

507   projected by CMIP5 DOD. However, the increase of DOD over the Middle East and the

508   decrease of DOD over northern China are similar to that of CMIP5 DOD. During JJA and

509   SON, DOD decreases over the Sahel and northern China but increases over a belt to the

510   north of central Sahel and parts of the Middle East (Figs. 9c-d). The weak increase of

511   DOD over the southern corner of South Africa in JJA and a slight decrease in SON also

512   has high agreement among the regression projections (dotted areas in Figs. 9c-d).

513   Changes of DOD over Australia are very small in all seasons and show little consistency

514   among the regression projections.

515   The regression model projection using 16-model output shows very similar

516   patterns (Figure S7 in the Supplement), largely because the projected changes of

517   precipitation, surface wind speed, and bareness from 16-model ensemble mean are

518   similar to those from 7-model ensemble mean in dusty regions (Figure S9 in the

519   Supplement). But there are also some discrepancies in terms of magnitude and pattern

520   that are revealed in the projected DOD patterns, e.g., the projected reduction of DOD is

521   greater and more widespread over the northern Asia in MAM if using 16-model output

522   and the increase of DOD along the southern edge of the Sahara is weaker in JJA and

523   SON (Fig. S7 in the Supplement vs. Fig. 9).

524   The contribution of each controlling factor to the total DOD change is shown in

525   Figure 10. While changes of bareness over North Africa and northern China play an

526   important role in DOD change, changes of precipitation, e.g. over northwestern China in

527   MAM, and surface wind, e.g., over northern North Africa and the Middle East in DJF and

528   MAM, also play vital roles.

529   Both projections from the CMIP5 models and that from the regression model have

530   some uncertainties. The reliability of future projection by CMIP5 models is limited by

531   models' capability of capturing present-day climatology and observed connection

532   between DOD and local controlling factors. As discussed earlier, the overall performance

533   of models is better in those very dusty regions in the NH, such as North Africa and the

534   Middle East, than other regions. Multi-model mean also overestimates the connection

535   between DOD and precipitation and surface wind and underestimates the influence of

536   bareness in the present-day (Fig. 6), which can cast doubts on the projected variation of

537   DOD in response to climate change.

538   The uncertainties associated with regression model are two folds. First, there're

539   uncertainties associated with the regression model itself. Since the regression coefficients

540   are derived from observed relationships between DOD and controlling factors in a

541   relatively short time period, factors controlling the low frequency variation of DOD (e.g.,

542   decadal variations) may not be included. Other meteorological factors that could play an

543   important role in regional dust variability, e.g., nocturnal low-level jets (e.g., Todd et al.,

544   2008; Fiedler et al., 2013; Fiedler et al., 2016) and haboobs over Africa (e.g., Ashpole

545   and Washington, 2013), are not directly considered in the model. The influences of

546   anthropogenic land use/land cover change are also not included in the regression model.

547   Anthropogenic land use/land cover change has been found to have played an important

548   role in long-term dust variability in some regions (e.g., Neff et al., 2005; 2008; Moulin

549   and Chiapello, 2006; McConnell et al., 2007), although previous modeling study found

550   its influences on future dust emission was minor compared to climate change (Tegen et

551   al., 2004). So the projection made by the regression model only reveals the change of

552   DOD in association with climate change. Second, uncertainties associated with model

553   projected change of controlling factors, such as bareness in U.S. in JJA as pointed by Pu

554   and Ginoux (2017), also limit the accuracy of the results.

555   Despite these uncertainties, both methods make similar projections particularly in

556   some dusty regions. For instance, the DOD pattern over North Africa in DJF and JJA, an

557   increase of DOD in the central Arabian Peninsula in all seasons, and a decrease of DOD

558   over northern China from MAM to SON (Figs. 7, 9).

559

560   **4. Discussion**

561   We examined DOD in seven CMIP5 models with interactive dust emission

562   schemes. Other important variables that influence the radiative property of dust, such as

563   Angström exponent and single scattering albedo, are also worth further examination, if

564   these variables are archived. A better quantification of the radiative forcing of dust may

565   also require an examination on the size distribution of dust particles, as studies (e.g., Kok

566   et al., 2017) found in current AeroCom models fraction of coarse dust particles were

567   underestimated and so was the warming effect of dust. Whether this is the case in the

568   CMIP5 models is not clear.

569   Also note that since DOD is an integrated variable, it does not reflect the vertical

570   distribution of dust aerosols. As pointed by Huneeus et al., (2016), dust models with

571   similar performance in simulating aerosol optical depth may have quite large differences

572   in simulating vertical distribution, emission, deposition, and surface concentration of

573   dust. An overall evaluation of dust modeling capability will require detailed examination

574   of these variables and the life cycle of dust in CMIP5 models in addition to DOD.

575   Early studies on future dust projection used offline dust models driven by climate

576   model output under different scenarios. For instance, Mahowald and Luo (2003) used an

577   offline dust model and output from National Center of Atmospheric Research's coupled

578   Climate System Model (CSM) 1.0 (Boville and Gent, 1998) under A1 scenario

579   (Houghton et al., 2001) and projected a decrease of dust emission by the end of the 21st

580   century by -20% to -63%, depending on different scenarios. In general, when they

581   included vegetation change, the projected dust reduction became greater, but including

582   land use change slightly weakened such reduction. Similarly, Tegen et al. (2004) used

583   output from ECHAM4 and HadCM3 and a dust model (Tegen et al., 2002) to examine

584   the change of dust emission by 2040-2050 and 2070-2080 and found results were model

585   and scenario dependent, from -26% to 10%. However, including anthropogenic

586   cultivation practices tended to increase dust emission in both models. They also pointed

587   out that such an influence from anthropogenic land-use was not big enough to overcome

588   the effect of climate change.

589   The interactive dust emission schemes and new generations of climate models

590   used in CMIP5 are likely to provide more reliable projections, but this may also depend

591   on how changes of dust and its radiative forcing are fed back to the climate system in the

592   models. While these projections are largely model-dependent, based on our analysis on

593   the DOD climatology in CMIP5 models, the multi-model mean has a better chance to

594   provide a more reliable projection than individual models.

595   Here a regression model combined with MODIS DOD is used to identify key

596   local factors that control the variation of DOD on the interannual time scale. The results

597   are then compared with model output to examine models' capability of capturing

598   observed connections between DOD and controlling factors. This method may be applied

599   to other dust model intercomparison projects as well, such as AeroCom (Huneeus et al.

600   2011), to help examine model performance.

601

602   **5. Conclusion**

603   Dust aerosol plays an important role in the climate system by directly scattering

604   and absorbing solar and longwave radiation and indirectly affecting the formation and

605   radiative properties of cloud. It is thus very important to understand how well dust is

606   simulated in the state-of-the-art climate models. While many features and variables are

607   systematically examined in the CMIP5 multi-model output, we found that to our best

608   knowledge an evaluation of global dust modeling in CMIP5 models is still in blank. In

609   this study we examined a key variable associated with dust radiative effect, dust optical

610   depth (DOD), using seven CMIP5 models with interactive dust emission schemes and

611   DOD retrieved from MODIS Deep Blue aerosol products.

612   We found that the global spatial pattern and magnitude are largely captured by

613   CMIP5 models in the 2004-2016 climatology, with an underestimation of global DOD

614   (over land) by -25.2% in MAM to -6.4% in DJF. The spatial pattern is better captured in

615   boreal dusty seasons during MAM and JJA. In JJA, the simulated zonal mean DOD from

616   multi-model mean largely resembles MODIS DOD.

617   The magnitudes of multi-model mean are closer to MODIS climatology than most

618   individual models and are largely within ± one order of magnitude of MODIS DOD in

619   the nine regions examined here (North Africa, the Middle East, northern China, North

620   America, India, southeastern Asia, South Africa, South America, and Australia; see Fig. 1

621   and Table 2 for domains). While some models underestimate DOD in North America and

622   South America by more than two orders of magnitude, a few also overestimate DOD in

623   Australia by more than one order of magnitude. Both the magnitude and spatial patterns

624   of DOD are better captured over North Africa and the Middle East than other regions.

625   The multi-model mean also largely captures the seasonal cycle of DOD in some

626   very dusty regions, such as North Africa and the Middle East. Seasonal variations in

627   North America and India are also generally captured by the multi-model mean, with the

628   modeled DOD peaking at approximately the same season as in MODIS DOD, but not so

629   in northern China and southeastern Asia. Seasonal cycles in those dusty regions in the

630   southern hemisphere is generally not well captured, with modeled DOD over South

631   Africa and South America peaking later than that in MODIS DOD but earlier in

632   Australia.

633   The interannual variations of DOD are not captured by most of the CMIP5

634   models during 2004-2016. Models also underestimate the constraints from surface

635   bareness on the variations of DOD and overestimate the influences from surface wind

636   speed and precipitation in those major dust source regions. CMIP5 model projected

637   change of DOD in the late half of the 21st century (under the RCP 8.5 scenario) with

638 reference to historical condition (1861-2005) also shows greater influence from

639 precipitation and surface wind change than from surface bareness. Overall, multi-model

640 mean projects a change of DOD over land from -3.8% in SON to 3.3% in JJA.

641   We also provide a projection of future DOD change using a regression model

642 based on local controlling factors such as surface wind, bareness, and precipitation (Pu

643 and Ginoux, 2017). This model can largely capture the interannual variations of MODIS

644 DOD in 2004-2016. The regression model projects a reduction of DOD in the Sahel in all

645 seasons in the late half of the 21st century under the RCP 8.5 scenario, largely due to a

646 decrease of surface bareness. DOD is projected to increase over the southern edge of the

647 Sahara in association with surface wind and precipitation changes except in MAM, when

648 a reduction of DOD over most part of North Africa is projected. DOD is also projected

649 to increase over the central Arabian Peninsula in all seasons and to decrease over

650 northern China from MAM to SON.

651   Despite large uncertainties associated with both projections, we find some

652 similarities between the two, which adds to the confidence of projected DOD change in

653 these regions, for instance, changes of DOD over North Africa in DJF and JJA, an

654 increase of DOD in the central Arabian Peninsula in all seasons, and a decrease of DOD

655 over northern China from MAM to SON.

656

657

658

659

660

661   *Acknowledgements.*

662   This research is supported by NOAA and Princeton University's Cooperative

663   Institute for Climate Science and NASA under grants NNH14ZDA001N-ACMAP and

664   NNH16ZDA001N-MAP. The authors thank Drs. Songmiao Fan and Fabien Paulot for

665   their helpful comments on the early version of this paper. The insightful comments from

666   two anonymous reviewers improved the paper.

667   PRECL Precipitation data are provided by the NOAA/OAR/ESRL PSD, Boulder,

668   Colorado, USA, from their web site at *http://www.esrl.noaa.gov/psd/*. The CALIOP

669   products are downloaded from *https://www-*

670   *calipso.larc.nasa.gov/tools/data_avail/dpo_read.php?y=2007&m=08&d=10*. AVHRR

671   leaf area index data are available at:

672   https://www.ngdc.noaa.gov/docucomp/page?xml=NOAA/NESDIS/NCDC/Geoportal/iso/

673   xml/C00898.xml&view=getDataView&header=none. The ERA-Interim is downloaded

674   from http://www.ecmwf.int/en/research/climate-reanalysis/era-interim. The AERONET

675   coarse mode aerosol optical depth data are downloaded from

676   https://aeronet.gsfc.nasa.gov/. CMIP5 data are downloaded from:

677   https://pcmdi.llnl.gov/projects/esgf-llnl/.

678

679

680

681

682

683

684   Reference
685
686 Abudu, S., Cui, C. L., King, J. P., Moreno, J., and Bawazir, A. S.: Modeling of daily pan

687   evaporation using partial least squares regression, Sci China Technol Sc, 54, 163-

688   174, 10.1007/s11431-010-4205-z, 2011.

689 Arora, V. K., Scinocca, J. F., Boer, G. J., Christian, J. R., Denman, K. L., Flato, G. M.,

690   Kharin, V. V., Lee, W. G., and Merryfield, W. J.: Carbon emission limits required

691   to satisfy future representative concentration pathways of greenhouse gases,

692   Geophys Res Lett, 38, 10.1029/2010gl046270, 2011.

693 Ashpole, I., and Washington, R.: A new high-resolution central and western Saharan

694   summertime dust source map from automated satellite dust plume tracking, J

695   Geophys Res-Atmos, 118, 6981-6995, 10.1002/jgrd.50554, 2013.

696 Baddock, M. C., Ginoux, P., Bullard, J. E., and Gill, T. E.: Do MODIS-defined dust

697   sources have a geomorphological signature?, Geophys Res Lett, 43, 2606-2613,

698   10.1002/2015gl067327, 2016.

699 Bangert, M., Nenes, A., Vogel, B., Vogel, H., Barahona, D., Karydis, V. A., Kumar, P.,

700   Kottmeier, C., and Blahak, U.: Saharan dust event impacts on cloud formation

701   and radiation over Western Europe, Atmos Chem Phys, 12, 4045-4063,

702   10.5194/acp-12-4045-2012, 2012.

703 Bellouin, N., Rae, J., Jones, A., Johnson, C., Haywood, J., and Boucher, O.: Aerosol

704   forcing in the Climate Model Intercomparison Project (CMIP5) simulations by

705   HadGEM2-ES and the role of ammonium nitrate, J Geophys Res-Atmos, 116,

706   10.1029/2011jd016074, 2011.

707   Bentsen, M., Bethke, I., Debernard, J. B., Iversen, T., Kirkevag, A., Seland, O., Drange,

708   H., Roelandt, C., Seierstad, I. A., Hoose, C., and Kristjansson, J. E.: The

709   Norwegian Earth System Model, NorESM1-M - Part 1: Description and basic

710   evaluation of the physical climate, Geosci Model Dev, 6, 687-720, 10.5194/gmd-

711   6-687-2013, 2013.

712   Boville, B. A., and Gent, P. R.: The NCAR Climate System Model, version one, J

713   Climate, 11, 1115-1130, Doi 10.1175/1520-

714   0442(1998)011<1115:Tncsmv>2.0.Co;2, 1998.

715   Chen, M. Y., Xie, P. P., Janowiak, J. E., and Arkin, P. A.: Global land precipitation: A

716   50-yr monthly analysis based on gauge observations, J Hydrometeorol, 3, 249-

717   266, Doi 10.1175/1525-7541(2002)003<0249:Glpaym>2.0.Co;2, 2002.

718   Claverie, M., Matthews, J. L., Vermote, E. F., and Justice, C. O.: A 30+ Year AVHRR

719   LAI and FAPAR Climate Data Record: Algorithm Description and Validation,

720   Remote Sens-Basel, 8, 10.3390/rs8030263, 2016.

721   Collins, W. J., Bellouin, N., Doutriaux-Boucher, M., Gedney, N., Halloran, P., Hinton,

722   T., Hughes, J., Jones, C. D., Joshi, M., Liddicoat, S., Martin, G., O'Connor, F.,

723   Rae, J., Senior, C., Sitch, S., Totterdell, I., Wiltshire, A., and Woodward, S.:

724   Development and evaluation of an Earth-System model-HadGEM2, Geosci

725   Model Dev, 4, 1051-1075, 10.5194/gmd-4-1051-2011, 2011.

726   Cook, B. I., Miller, R. L., and Seager, R.: Dust and sea surface temperature forcing of the

727   1930s "Dust Bowl" drought, Geophys Res Lett, 35, 10.1029/2008gl033486, 2008.

728   Cook, B. I., Miller, R. L., and Seager, R.: Amplification of the North American "Dust

729   Bowl" drought through human-induced land degradation, P Natl Acad Sci USA,

730   106, 4997-5001, 10.1073/pnas.0810200106, 2009.

731   Cook, B. I., Seager, R., Miller, R. L., and Mason, J. A.: Intensification of North

732   American Megadroughts through Surface and Dust Aerosol Forcing, J Climate,

733   26, 4414-4430, 10.1175/Jcli-D-12-00022.1, 2013.

734   Croft, B., Lohmann, U., and von Salzen, K.: Black carbon ageing in the Canadian Centre

735   for Climate modelling and analysis atmospheric general circulation model, Atmos

736   Chem Phys, 5, 1931-1949, 2005.

737   Donner, L. J., Wyman, B. L., Hemler, R. S., Horowitz, L. W., Ming, Y., Zhao, M., Golaz,

738   J. C., Ginoux, P., Lin, S. J., Schwarzkopf, M. D., Austin, J., Alaka, G., Cooke, W.

739   F., Delworth, T. L., Freidenreich, S. M., Gordon, C. T., Griffies, S. M., Held, I.

740   M., Hurlin, W. J., Klein, S. A., Knutson, T. R., Langenhorst, A. R., Lee, H. C.,

741   Lin, Y. L., Magi, B. I., Malyshev, S. L., Milly, P. C. D., Naik, V., Nath, M. J.,

742   Pincus, R., Ploshay, J. J., Ramaswamy, V., Seman, C. J., Shevliakova, E., Sirutis,

743   J. J., Stern, W. F., Stouffer, R. J., Wilson, R. J., Winton, M., Wittenberg, A. T.,

744   and Zeng, F. R.: The Dynamical Core, Physical Parameterizations, and Basic

745   Simulation Characteristics of the Atmospheric Component AM3 of the GFDL

746   Global Coupled Model CM3, J Climate, 24, 3484-3519, 10.1175/2011jcli3955.1,

747   2011.

748   Dunion, J. P., and Velden, C. S.: The impact of the Saharan air layer on Atlantic tropical

749   cyclone activity, B Am Meteorol Soc, 85, 353-+, 10.1175/Bams-85-3-353, 2004.

750   Evan, A. T., Dunion, J., Foley, J. A., Heidinger, A. K., and Velden, C. S.: New evidence

751   for a relationship between Atlantic tropical cyclone activity and African dust

752   outbreaks, Geophys Res Lett, 33, 10.1029/2006gl026408, 2006.

753   Evan, A. T., and Mukhopadhyay, S.: African Dust over the Northern Tropical Atlantic:

754   1955-2008, J Appl Meteorol Clim, 49, 2213-2229, 10.1175/2010jamc2485.1,

755   2010.

756   Evan, A. T., Flamant, C., Fiedler, S., and Doherty, O.: An analysis of aeolian dust in

757   climate models, Geophys Res Lett, 41, 5996-6001, 10.1002/2014gl060545, 2014.

758   Evan, A. T., Flamant, C., Gaetani, M., and Guichard, F.: The past, present and future of

759   African dust, Nature, 531, 493-+, 10.1038/nature17149, 2016.

760   Evans, S., Ginoux, P., Malyshev, S., and Shevliakova, E.: Climate-vegetation interaction

761   and amplification of Australian dust variability, Geophys Res Lett, 43, 11823-

762   11830, 10.1002/2016gl071016, 2016.

763   Fecan, F., Marticorena, B., and Bergametti, G.: Parametrization of the increase of the

764   aeolian erosion threshold wind friction velocity due to soil moisture for arid and

765   semi-arid   areas,   Ann   Geophys-Atm   Hydr,   17,   149-157,   DOI

766   10.1007/s005850050744, 1999.

767   Fiedler, S., Schepanski, K., Heinold, B., Knippertz, P., and Tegen, I.: Climatology of

768   nocturnal low-level jets over North Africa and implications for modeling mineral

769   dust emission, J Geophys Res-Atmos, 118, 6100-6121, 10.1002/jgrd.50394, 2013.

770   Fiedler, S., Knippertz, P., Woodward, S., Martin, G. M., Bellouin, N., Ross, A. N.,

771   Heinold, B., Schepanski, K., Birch, C. E., and Tegen, I.: A process-based

evaluation of dust-emitting winds in the CMIP5 simulation of HadGEM2-ES, Clim Dynam, 46, 1107-1130, 10.1007/s00382-015-2635-9, 2016.

Fung, I. Y., Meyn, S. K., Tegen, I., Doney, S. C., John, J. G., and Bishop, J. K. B.: Iron supply and demand in the upper ocean, Global Biogeochem Cy, 14, 281-295, Doi 10.1029/1999gb900059, 2000.

Fuss, S., Canadell, J. G., Peters, G. P., Tavoni, M., Andrew, R. M., Ciais, P., Jackson, R. B., Jones, C. D., Kraxner, F., Nakicenovic, N., Le Quere, C., Raupach, M. R., Sharifi, A., Smith, P., and Yamagata, Y.: COMMENTARY: Betting on negative emissions, Nat Clim Change, 4, 850-853, DOI 10.1038/nclimate2392, 2014.

Gillette, D. A., and Passi, R.: Modeling Dust Emission Caused by Wind Erosion, J Geophys Res-Atmos, 93, 14233-14242, DOI 10.1029/JD093iD11p14233, 1988.

Ginoux, P., Chin, M., Tegen, I., Prospero, J. M., Holben, B., Dubovik, O., and Lin, S. J.: Sources and distributions of dust aerosols simulated with the GOCART model, J Geophys Res-Atmos, 106, 20255-20273, Doi 10.1029/2000jd000053, 2001.

Ginoux, P., Garbuzov, D., and Hsu, N. C.: Identification of anthropogenic and natural dust sources using Moderate Resolution Imaging Spectroradiometer (MODIS) Deep Blue level 2 data, J Geophys Res-Atmos, 115, 10.1029/2009jd012398, 2010.

Ginoux, P., Clarisse, L., Clerbaux, C., Coheur, P. F., Dubovik, O., Hsu, N. C., and Van Damme, M.: Mixing of dust and NH3 observed globally over anthropogenic dust sources, Atmos Chem Phys, 12, 7351-7363, 10.5194/acp-12-7351-2012, 2012a.

Ginoux, P., Prospero, J. M., Gill, T. E., Hsu, N. C., and Zhao, M.: Global-Scale Attribution of Anthropogenic and Natural Dust Sources and Their Emission Rates

795   Based on MODIS Deep Blue Aerosol Products, Rev Geophys, 50,

796   10.1029/2012rg000388, 2012b.

797   Houghton, J., Ding, Y., Griggs, D. J., Noguer, M., Linden, P. J. v. d., Dai, X., Maskell,

798   K., and Johnson, C. A.: Climate Change 2001: The scientific basis. Contribution

799   of Working Group I to the Third Assessment Report of the Intergovernmental

800   Panel on Climate Change, in, Cambridge Univ. Press, Cambridge, UK, 2001.

801   Hsu, N. C., Tsay, S. C., King, M. D., and Herman, J. R.: Aerosol properties over bright-

802   reflecting source regions, Ieee T Geosci Remote, 42, 557-569,

803   10.1109/Tgrs.2004.824067, 2004.

804   Hsu, N. C., Tsay, S. C., King, M. D., and Herman, J. R.: Deep blue retrievals of Asian

805   aerosol properties during ACE-Asia, Ieee T Geosci Remote, 44, 3180-3195,

806   10.1109/Tgrs.2006.879540, 2006.

807   Hsu, N. C., Jeong, M. J., Bettenhausen, C., Sayer, A. M., Hansell, R., Seftor, C. S.,

808   Huang, J., and Tsay, S. C.: Enhanced Deep Blue aerosol retrieval algorithm: The

809   second generation, J Geophys Res-Atmos, 118, 9296-9315, 10.1002/jgrd.50712,

810   2013.

811   Huneeus, N., Schulz, M., Balkanski, Y., Griesfeller, J., Prospero, J., Kinne, S., Bauer, S.,

812   Boucher, O., Chin, M., Dentener, F., Diehl, T., Easter, R., Fillmore, D., Ghan, S.,

813   Ginoux, P., Grini, A., Horowitz, L., Koch, D., Krol, M. C., Landing, W., Liu, X.,

814   Mahowald, N., Miller, R., Morcrette, J. J., Myhre, G., Penner, J., Perlwitz, J.,

815   Stier, P., Takemura, T., and Zender, C. S.: Global dust model intercomparison in

816   AeroCom phase I, Atmos Chem Phys, 11, 7781-7816, 10.5194/acp-11-7781-

817   2011, 2011.

818   Jickells, T. D., An, Z. S., Andersen, K. K., Baker, A. R., Bergametti, G., Brooks, N., Cao,

819   J. J., Boyd, P. W., Duce, R. A., Hunter, K. A., Kawahata, H., Kubilay, N.,

820   laRoche, J., Liss, P. S., Mahowald, N., Prospero, J. M., Ridgwell, A. J., Tegen, I.,

821   and Torres, R.: Global iron connections between desert dust, ocean

822   biogeochemistry, and climate, Science, 308, 67-71, DOI

823   10.1126/science.1105959, 2005.

824   Jin, Q., Wei, J., Yang, Z. L., Pu, B., and Huang, J.: Consistent response of Indian summer

825   monsoon to Middle East dust in observations and simulations, Atmos Chem Phys,

826   15, 9897-9915, 10.5194/acp-15-9897-2015, 2015.

827   Jin, Q. J., Wei, J. F., and Yang, Z. L.: Positive response of Indian summer rainfall to

828   Middle East dust, Geophys Res Lett, 41, 4068-4074, 10.1002/2014gl059980,

829   2014.

830   Jin, Q. J., Yang, Z. L., and Wei, J. F.: Seasonal Responses of Indian Summer Monsoon to

831   Dust Aerosols in the Middle East, India, and China, J Climate, 29, 6329-6349,

832   10.1175/Jcli-D-15-0622.1, 2016.

833   Kim, M. K., Lau, W. K. M., Kim, K. M., Sang, J., Kim, Y. H., and Lee, W. S.:

834   Amplification of ENSO effects on Indian summer monsoon by absorbing

835   aerosols, Clim Dynam, 46, 2657-2671, 10.1007/s00382-015-2722-y, 2016.

836   Kok, J. F., Ridley, D. A., Zhou, Q., Miller, R. L., Zhao, C., Heald, C. L., Ward, D. S.,

837   Albani, S., and Haustein, K.: Smaller desert dust cooling effect estimated from

838   analysis of dust size and abundance, Nat Geosci, 10, 274-+, 10.1038/Ngeo2912,

839   2017.

840 Laurent, B., Marticorena, B., Bergametti, G., and Mei, F.: Modeling mineral dust

841   emissions from Chinese and Mongolian deserts, Global Planet Change, 52, 121-

842   141, 10.1016/j.gloplacha.2006.02.012, 2006.

843 Levin, Z., Ganor, E., and Gladstein, V.: The effects of desert particles coated with sulfate

844   on rain formation in the eastern Mediterranean, J Appl Meteorol, 35, 1511-1523,

845   Doi 10.1175/1520-0450(1996)035<1511:Teodpc>2.0.Co;2, 1996.

846 Mahowald, N. M., and Luo, C.: A less dusty future?, Geophys Res Lett, 30,

847   10.1029/2003gl017880, 2003.

848 Mahowald, N. M., Kloster, S., Engelstaedter, S., Moore, J. K., Mukhopadhyay, S.,

849   McConnell, J. R., Albani, S., Doney, S. C., Bhattacharya, A., Curran, M. A. J.,

850   Flanner, M. G., Hoffman, F. M., Lawrence, D. M., Lindsay, K., Mayewski, P. A.,

851   Neff, J., Rothenberg, D., Thomas, E., Thornton, P. E., and Zender, C. S.:

852   Observed 20th century desert dust variability: impact on climate and

853   biogeochemistry, Atmos Chem Phys, 10, 10875-10893, 10.5194/acp-10-10875-

854   2010, 2010.

855 Marticorena, B., and Bergametti, G.: Modeling the Atmospheric Dust Cycle .1. Design of

856   a Soil-Derived Dust Emission Scheme, J Geophys Res-Atmos, 100, 16415-16430,

857   Doi 10.1029/95jd00690, 1995.

858 Marx, S. K., McGowan, H. A., and Kamber, B. S.: Long-range dust transport from

859   eastern Australia: A proxy for Holocene aridity and ENSO-type climate

860   variability, Earth Planet Sc Lett, 282, 167-177, 10.1016/j.epsl.2009.03.013, 2009.

861 McConnell, J. R., Aristarain, A. J., Banta, J. R., Edwards, P. R., and Simoes, J. C.: 20th-

862   Century doubling in dust archived in an Antarctic Peninsula ice core parallels

863   climate change and desertification in South America, P Natl Acad Sci USA, 104,

864   5743-5748, 10.1073/pnas.0607657104, 2007.

865   Miller, R. L., and Tegen, I.: Climate response to soil dust aerosols, J Climate, 11, 3247-

866   3267, Doi 10.1175/1520-0442(1998)011<3247:Crtsda>2.0.Co;2, 1998.

867   Miller, R. L., Tegen, I., and Perlwitz, J.: Surface radiative forcing by soil dust aerosols

868   and the hydrologic cycle, J Geophys Res-Atmos, 109, 10.1029/2003jd004085,

869   2004.

870   Misra, A., Kanawade, V. P., and Tripathi, S. N.: Quantitative assessment of AOD from

871   17 CMIP5 models based on satellite-derived AOD over India, Ann Geophys-

872   Germany, 34, 657-671, 10.5194/angeo-34-657-2016, 2016.

873   Moulin, C., and Chiapello, I.: Impact of human-induced desertification on the

874   intensification of Sahel dust emission and export over the last decades, Geophys

875   Res Lett, 33, 10.1029/2006gl025923, 2006.

876   Myhre, G., Shindell, D., Bréon, F.-M., Collins, W., Fuglestvedt, J., Huang, J., Koch, D.,

877   Lamarque, J.-F., Lee, D., Mendoza, B., Nakajima, T., Robock, A., Stephens, G.,

878   Takemura, T., and Zhang, H.: Anthropogenic and Natural Radiative Forcing. , in:

879   Climate Change 2013: The Physical Science Basis. Contribution of Working

880   Group I to the Fifth Assessment Report of the Intergovernmental Panel on

881   Climate Change, edited by: Stocker, T. F., Qin, D., Plattner, G.-K., Tignor, M.,

882   Allen, S. K., Boschung, J., Nauels, A., Xia, Y., Bex, V., and Midgley, P. M.,

883   Cambridge University Press, Cambridge, United Kingdom and New York, NY,

884   USA, 2013.

885 Nakajima, T., Higurashi, A., Kawamoto, K., and Penner, J. E.: A possible correlation
886   between satellite-derived cloud and aerosol microphysical parameters, Geophys
887   Res Lett, 28, 1171-1174, Doi 10.1029/2000gl012186, 2001.

888 Neff, J. C., Reynolds, R. L., Belnap, J., and Lamothe, P.: Multi-decadal impacts of
889   grazing on soil physical and biogeochemical properties in southeast Utah, Ecol
890   Appl, 15, 87-95, Doi 10.1890/04-0268, 2005.

891 Neff, J. C., Ballantyne, A. P., Farmer, G. L., Mahowald, N. M., Conroy, J. L., Landry, C.
892   C., Overpeck, J. T., Painter, T. H., Lawrence, C. R., and Reynolds, R. L.:
893   Increasing eolian dust deposition in the western United States linked to human
894   activity, Nat Geosci, 1, 189-195, 10.1038/ngeo133, 2008.

895 O'Brien, R. M.: A caution regarding rules of thumb for variance inflation factors, Qual
896   Quant, 41, 673-690, 10.1007/s11135-006-9018-6, 2007.

897 O'Neill, N. T., Eck, T. F., Smirnov, A., Holben, B. N., and Thulasiraman, S.: Spectral
898   discrimination of coarse and fine mode optical depth, J Geophys Res-Atmos, 108,
899   10.1029/2002jd002975, 2003.

900 Prospero, J. M., and Nees, R. T.: Impact of the North African Drought and El-Nino on
901   Mineral Dust in the Barbados Trade Winds, Nature, 320, 735-738, DOI
902   10.1038/320735a0, 1986.

903 Prospero, J. M., and Lamb, P. J.: African droughts and dust transport to the Caribbean:
904   Climate change implications, Science, 302, 1024-1027, DOI
905   10.1126/science.1089915, 2003.

906   Pu, B., Fu, R., Dickinson, R. E., and Fernando, D. N.: Why do summer droughts in the
907   Southern Great Plains occur in some La Nina years but not others?, J Geophys
908   Res-Atmos, 121, 1120-1137, 10.1002/2015jd023508, 2016.

909   Pu, B., and Ginoux, P.: The impact of the Pacific Decadal Oscillation on springtime dust
910   activity in Syria, Atmos Chem Phys, 16, 13431-13448, 10.5194/acp-16-13431-
911   2016, 2016.

912   Pu, B., and Ginoux, P.: Projection of American dustiness in the late 21st century due to
913   climate change, Scientific reports, 7, 10.1038/s41598-017-05431-9, 2017.

914   Reader, M. C., Fung, I., and McFarlane, N.: The mineral dust aerosol cycle during the
915   last glacial maximum (vol 104, pg 9381, 1999), J Geophys Res-Atmos, 104,
916   22319-22320, Doi 10.1029/1999jd900434, 1999.

917   Riahi, K., Rao, S., Krey, V., Cho, C. H., Chirkov, V., Fischer, G., Kindermann, G.,
918   Nakicenovic, N., and Rafaj, P.: RCP 8.5-A scenario of comparatively high
919   greenhouse gas emissions, Climatic Change, 109, 33-57, 10.1007/s10584-011-
920   0149-y, 2011.

921   Rosenfield, J. E., Considine, D. B., Meade, P. E., Bacmeister, J. T., Jackman, C. H., and
922   Schoeberl, M. R.: Stratospheric effects of Mount Pinatubo aerosol studied with a
923   coupled two-dimensional model, J Geophys Res-Atmos, 102, 3649-3670, Doi
924   10.1029/96jd03820, 1997.

925   Sanap, S. D., Ayantika, D. C., Pandithurai, G., and Niranjan, K.: Assessment of the
926   aerosol distribution over Indian subcontinent in CMIP5 models, Atmospheric
927   Environment, 87, 123-137, 10.1016/j.atmosenv.2014.01.017, 2014.

928   Seland, O., Iversen, T., Kirkevag, A., and Storelvmo, T.: Aerosol-climate interactions in

929   the CAM-Oslo atmospheric GCM and investigation of associated basic

930   shortcomings, Tellus A, 60, 459-491, 10.1111/j.1600-0870.2008.00318.x, 2008.

931   Shao, Y. P., Wyrwoll, K. H., Chappell, A., Huang, J. P., Lin, Z. H., McTainsh, G. H.,

932   Mikami, M., Tanaka, T. Y., Wang, X. L., and Yoon, S.: Dust cycle: An emerging

933   core theme in Earth system science, Aeolian Res, 2, 181-204,

934   10.1016/j.aeolia.2011.02.001, 2011.

935   Sharma, D., and Miller, R. L.: Revisiting the observed correlation between weekly

936   averaged Indian monsoon precipitation and Arabian Sea aerosol optical depth,

937   Geophys Res Lett, 44, 10006-10016, 10.1002/2017gl074373, 2017.

938   Shindell, D. T., Lamarque, J. F., Schulz, M., Flanner, M., Jiao, C., Chin, M., Young, P. J.,

939   Lee, Y. H., Rotstayn, L., Mahowald, N., Milly, G., Faluvegi, G., Balkanski, Y.,

940   Collins, W. J., Conley, A. J., Dalsoren, S., Easter, R., Ghan, S., Horowitz, L., Liu,

941   X., Myhre, G., Nagashima, T., Naik, V., Rumbold, S. T., Skeie, R., Sudo, K.,

942   Szopa, S., Takemura, T., Voulgarakis, A., Yoon, J. H., and Lo, F.: Radiative

943   forcing in the ACCMIP historical and future climate simulations, Atmos Chem

944   Phys, 13, 2939-2974, 10.5194/acp-13-2939-2013, 2013.

945   Solmon, F., Nair, V. S., and Mallet, M.: Increasing Arabian dust activity and the Indian

946   summer monsoon, Atmos Chem Phys, 15, 8051-8064, 10.5194/acp-15-8051-

947   2015, 2015.

948   Strong, J. D., Vecchi, G. A., and Ginoux, P.: The Climatological Effect of Saharan Dust

949   on Global Tropical Cyclones in a Fully Coupled GCM, Journal of Geophysical

950   Research - Atmospheres, 123, https://doi.org/10.1029/2017JD027808, 2018.

951   Strong, J. D. O., Vecchi, G. A., and Ginoux, P.: The Response of the Tropical Atlantic

952   and West African Climate to Saharan Dust in a Fully Coupled GCM, J Climate,

953   28, 7071-7092, 10.1175/Jcli-D-14-00797.1, 2015.

954   Sun, D. L., Lau, K. M., and Kafatos, M.: Contrasting the 2007 and 2005 hurricane

955   seasons: Evidence of possible impacts of Saharan dry air and dust on tropical

956   cyclone   activity   in   the   Atlantic   basin,   Geophys   Res   Lett,   35,

957   10.1029/2008gl034529, 2008.

958   Takemura, T., Okamoto, H., Maruyama, Y., Numaguti, A., Higurashi, A., and Nakajima,

959   T.: Global three-dimensional simulation of aerosol optical thickness distribution

960   of   various   origins,   J   Geophys   Res-Atmos,   105,   17853-17873,   Doi

961   10.1029/2000jd900265, 2000.

962   Tegen, I., Harrison, S. P., Kohfeld, K., Prentice, I. C., Coe, M., and Heimann, M.: Impact

963   of vegetation and preferential source areas on global dust aerosol: Results from a

964   model study, J Geophys Res-Atmos, 107, 10.1029/2001jd000963, 2002.

965   Tegen, I., Werner, M., Harrison, S. P., and Kohfeld, K. E.: Relative importance of

966   climate and land use in determining present and future global soil dust emission,

967   Geophys Res Lett, 31, 10.1029/2003gl019216, 2004.

968   Todd, M. C., Washington, R., Raghavan, S., Lizcano, G., and Knippertz, P.: Regional

969   model simulations of the Bodele low-level jet of northern Chad during the Bodele

970   Dust   Experiment   (BoDEx   2005),   J   Climate,   21,   995-1012,

971   10.1175/2007jcli1766.1, 2008.

972 Vinoj, V., Rasch, P. J., Wang, H. L., Yoon, J. H., Ma, P. L., Landu, K., and Singh, B.:

973   Short-term modulation of Indian summer monsoon rainfall by West Asian dust,

974   Nat Geosci, 7, 308-313, 10.1038/ngeo2107, 2014.

975 Watanabe, S., Hajima, T., Sudo, K., Nagashima, T., Takemura, T., Okajima, H., Nozawa,

976   T., Kawase, H., Abe, M., Yokohata, T., Ise, T., Sato, H., Kato, E., Takata, K.,

977   Emori, S., and Kawamiya, M.: MIROC-ESM 2010: model description and basic

978   results of CMIP5-20c3m experiments, Geosci Model Dev, 4, 845-872,

979   10.5194/gmd-4-845-2011, 2011.

980 Winker, D. M., Hunt, W., and Hostetler, C.: Status and performance of the CALIOP

981   lidar, Bba Lib, 5575, 8-15, 10.1117/12.571955, 2004.

982 Winker, D. M., Hunt, W. H., and McGill, M. J.: Initial performance assessment of

983   CALIOP, Geophys Res Lett, 34, 10.1029/2007gl030135, 2007.

984 Wong, S., and Dessler, A. E.: Suppression of deep convection over the tropical North

985   Atlantic by the Saharan Air Layer, Geophys Res Lett, 32, 10.1029/2004gl022295,

986   2005.

987 Wurzler, S., Reisin, T. G., and Levin, Z.: Modification of mineral dust particles by cloud

988   processing and subsequent effects on drop size distributions, J Geophys Res-

989   Atmos, 105, 4501-4512, Doi 10.1029/1999jd900980, 2000.

990 Zender, C. S., and Kwon, E. Y.: Regional contrasts in dust emission responses to climate,

991   J Geophys Res-Atmos, 110, 10.1029/2004jd005501, 2005.

992 Zhao, T. L., Gong, S. L., Zhang, X. Y., Blanchet, J. P., McKendry, I. G., and Zhou, Z. J.:

993   A simulated climatology of Asian dust aerosol and its trans-Pacific transport. Part

994   I: Mean climate and validation, J Climate, 19, 88-103, Doi 10.1175/Jcli3605.1,

995   2006.

996

997

998

999   Table 1 CMIP5 models used in this study. Models tagged with plus signs (+) included

1000   anthropogenic land use/land cover change in their vegetation prediction.

1001

1002   Table 2 List of regions selected to compare model output with MODIS DOD. Locations

1003   of these regions are also plotted in Fig. 1b. Acronyms are used for some regions for short,

1004   and are listed in the brackets in the first column. Note that the region names such as

1005   Northern China and India are not exactly the same as their geographical definitions but

1006   also covers some areas from nearby countries.

1007

1008   Table 3 Changes of DOD in the late half of the 21st century (2051-2100; RCP 8.5

1009   scenario) from the historical condition (1861-2005) projected by CMIP5 multi-model

1010   mean (second to fifth columns) and the regression model (sixth to ninth columns) in the

1011   nine regions. Changes of DOD are shown in percentage with reference to CMIP5 multi-

1012   model historical run. Note that in some regions the projected change by the regression

1013   model is quite large (i.e., greater than ± 100%), largely due to the underestimation of

1014   CMIP5 historical run in these regions.

1015

1016

1017

1018

1019

1020

1021

1022   Figure 1. Figure 1. Climatology (2004-2016) of Aqua and Terra combined DOD (i.e.,

1023   MODIS DOD; top panel) and multi-model mean of CMIP5 DOD (bottom) for four

1024   seasons. The pattern correlation (centered; calculated after interpolating MODIS DOD to

1025   CMIP5 DOD grids) between CMIP5 and MODIS DOD are shown in pink in the bottom

1026   panel. Blue numbers denote global mean DOD over land. For CMIP5 model results, ±

1027   one standard deviation among seven CMIP5 models is also shown. Black boxes in (b)

1028   denote nine averaging regions (Table 2). Here we only added these boxes in (b) instead of

1029   every plot to keep the figure clean. Note that CMIP5 multi-model mean is masked by

1030   MODIS DOD for comparison. Dotted area in (e)-(h) shows where multi-model mean is

1031   greater than one inter-model standard deviation.

1032

1033   Figure 2. Zonal mean DOD from MODIS (thick red), CMIP5 multi-model mean (thick

1034   black), and each individual model (other colorful lines).

1035

1036   Figure 3. Seasonal cycle of DOD in nine regions (Table 2) averaged over 2004-2016.

1037   Thick red lines denote MODIS DOD, thick black lines denote CMIP5 multi-model mean,

1038   and other colorful lines denote individual model output. The annual means from MODIS

1039   DOD (Obs; red) and multi-model mean (Ens; black) are shown in each panel. Note that in

1040   (i) MODIS DOD (red line) is scaled ten times to better display the season cycle.

1041

1042   Figure 4. Spatial statistics comparing DOD from CMIP5 models with that from MODIS

1043   in nine regions. Label on the X-axis shows individual models (1-7) and multi-model

1044   mean (8). Y-axis shows the ratio of pattern standard deviations between model

1045   climatology (2004-2016) and that of MODIS, which reveals the relative amplitude of the

1046   simulated DOD versus satellite DOD. The color denotes pattern correlation (centered)

1047   between each model and MODIS DOD in each region.

1048

1049   Figure 5. Correlations (color) between regional averaged time series from CMIP5 DOD

1050   and MODIS DOD from 2004 to 2016 for four seasons. Numbers in the X-axis denotes

1051   each model (1-7) and multi-model mean (8). Correlations significant at the 90%

1052   confidence level are marked by a star and significance at the 95% confidence level by

1053   two stars.

1054

1055   Figure 6. Regression coefficients calculated by regressing DOD in each season onto

1056   standardized precipitation (purple), bareness (orange), and surface wind speed (green)

1057   from 2004 to 2016. Coefficients obtained using MODIS DOD and observed controlling

1058   factors (interpolated to a 2° by 2.5° grid) and those using CMIP5 multi-model mean DOD

1059   and controlling factors are shown in the left and right columns, respectively. The color of

1060   the shading denotes the largest coefficient in absolute value among the three, while the

1061   saturation of the color shows the magnitude of the coefficient (from 0 to 0.02). Only

1062   regression coefficients significant at the 90% confidence level (Bootstrap test) are shown.

1063   Missing values are shaded in grey. To highlight coefficients near the source regions, a

1064   mask of LAI ≤ 0.5 is applied.

1065

1066   Figure 7. Projected changes of DOD in the late half of the 21st century (under the RCP

1067   8.5 scenario) from that in the historical level (1861-2005) by CMIP5 multi-model mean

1068 for four seasons. The percentage change of global mean (over land) DOD ± one inter-

1069 model standard deviation is shown at the bottom of each plot. Areas with sign agreement

1070 among the models reaches 71.4% (i.e., at least five out of seven models have the same

1071 sign as the multi-model mean) are dotted.

1072

1073 Figure 8. Projected difference of (a)-(d) precipitation (mm day-1), (e)-(h) bareness, and

1074 (i)-(l) 10 m wind (m s-1) between the late half of the 21st century (2051-2100; RCP 8.5

1075 scenario) and historical level (1861-2005) from multi-model mean of seven CMIP5

1076 models. Areas with sign agreement among the models reaches 71.4% (i.e., at least five

1077 out of seven models have the same sign as the multi-model mean) are dotted.

1078

1079 Figure 9. Projected change of DOD in the late half of the 21st century under the RCP 8.5

1080 scenario by the regression model. The results are calculated using the regression

1081 coefficients obtained from observations during 2004-2016 (see methodology) and

1082 projected changes of precipitation, bareness, and surface wind from seven CMIP5

1083 models. Dotted areas are regions with sign agreement among the regression projections

1084 (using output of each of the seven models) above 71.4% (i.e., at least five out of seven

1085 regression projections have the same sign as the multi-model mean projection). To

1086 highlight DOD variations near the source regions, a mask of LAI ≤ 0.5 (from present-day

1087 climatology) is applied.

1088

1089 Figure 10. (a)-(d) Projected change of DOD in the late half of the 21st century under the

1090 RCP 8.5 scenario by the regression model and output from seven CMIP5 models (same

1091 as Fig. 9), and contributions from each component, (e)-(h) precipitation, (j)-(i) bareness,

1092 and (m)-(p) surface wind speed. Dotted areas are regions with sign agreement among the

1093 models above 71.4%. To highlight DOD variations near the source regions, a mask of

1094 LAI ≤ 0.5 (from present-day climatology) is applied.

1095

1096

1097

1098

1099

1100

1101

1102

1103

1104

1105

1106

1107

1108

1109

1110

1111

1112

1113

1114
1115   Table 1 CMIP5 models used in this study. Models tagged with plus signs (+) included
1116   anthropogenic land use/land cover change in their vegetation prediction.
1117

Model	lat/lon resolution	Dust emission implementation	Dynamic Vegetation	Model reference
CanESM2	2.8°×2.8°	Reader et al. (1999); Croft et al. (2005)	N[+]	Arora et al. (2011)
GFDL-CM3	2.0°×2.5°	Ginoux et al. (2001)	Y[+]	Donner et al. (2011)
HadGEM2-CC	1.2°×1.8°	Marticorena and Bergametti (1995)	Y[+]	Collins et al. (2011)
HadGEM2-ES	1.2°×1.8°	Marticorena and Bergametti (1995)	Y[+]	Collins et al. (2011)
MIROC-ESM	2.8°×2.8°	Takemura et al. (2000)	Y[+]	Watanabe et al. (2011)
MIROC-ESM-CHEM	2.8°×2.8°	Takemura et al. (2000)	Y[+]	Watanabe et al. (2011)
NorESM1-M	1.9°×2.5°	Seland et al. (2008)	N[+]	Bentsen et al. (2013)

1118
1119
1120
1121
1122
1123
1124
1125
1126
1127
1128
1129
1130
1131
1132
1133
1134
1135
1136
1137
1138
1139
1140
1141
1142
1143
1144
1145
1146
1147

1148

1149 Table 2 List of regions selected to compare model output with MODIS DOD. Locations
1150 of these regions are also plotted in Fig. 1b. Acronyms are used for some regions for short,
1151 and are listed in the brackets in the first column. Note that the region names such as
1152 northern China and India are not exactly the same as their geographical definitions but
1153 also cover some areas from nearby countries.

1154

Region	Domain
North Africa (N. Africa)	5°-50°N, 18°W-35°E
Middle East	12°-50°N, 35°-60°E
Northern China (N. China)	35°-50°N, 70°-110°E
North America (N. America)	25°-50°N, 95°-125°W
India	5°-35°N, 60°-90°E
Southeastern Asia (SE. Asia)	9°-35°N, 90°-121°E
South Africa (S. Africa)	15°-35°S, 10°-50°N
South America (S. America)	0°-55°S, 60°-83°W
Australia	10°-40°S, 112°-155°E

1155
1156
1157
1158
1159
1160
1161
1162
1163
1164
1165
1166
1167
1168
1169
1170
1171
1172
1173
1174
1175
1176
1177
1178
1179
1180
1181
1182
1183

1184

1185   Table 3 Changes of DOD in the late half of the 21st century (2051-2100; RCP 8.5
1186   scenario) from the historical condition (1861-2005) projected by CMIP5 multi-model
1187   mean (second to fifth columns) and the regression model (sixth to ninth columns) in nine
1188   regions. Changes of DOD are shown in percentage with reference to CMIP5 multi-model
1189   historical run. Note that in some regions the projected change by the regression model is
1190   quite large (i.e., greater than ± 100%), largely due to the underestimation of CMIP5
1191   historical run in these regions.

1192

Region	CMIP5				Regression model			
	DJF	MAM	JJA	SON	DJF	MAM	JJA	SON
N. Africa	-3.8	-3.6	2.4	-16.3	-0.8	-17.7	11.1	-10.3
Middle East	7.8	4.5	6.4	1.5	9.8	-16.0	-5.4	-8.4
N. China	-33.5	-11.4	-9.8	-14.4	312.3	-238.6	-51.2	-30.0
N. America	42.6	26.8	13.2	-6.4	-38.5	-90.0	9.3	-42.4
India	-5.1	0.2	-1.0	-9.9	-27.6	-8.2	-2.9	-32.3
SE. Asia	-45.7	-16.5	-13.5	-17.1	-34.8	1.6	4.2	96.3
S. Africa	24.0	6.1	38.5	54.4	22.3	59.3	231.8	78.3
S. America	35.7	27.4	51.8	36.0	14.8	56.1	78.3	154.6
Australia	-3.2	-3.2	15.3	17.0	2.7	0.4	0.7	3.7

1193
1194
1195
1196
1197
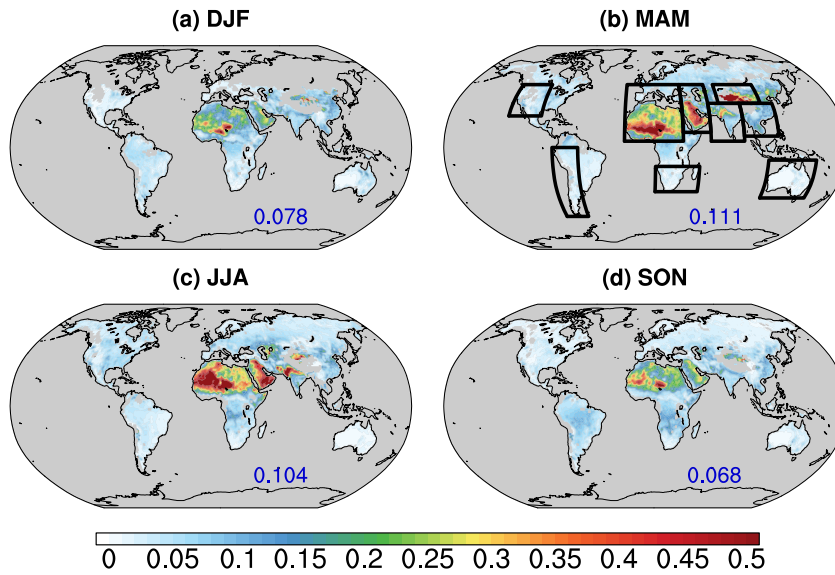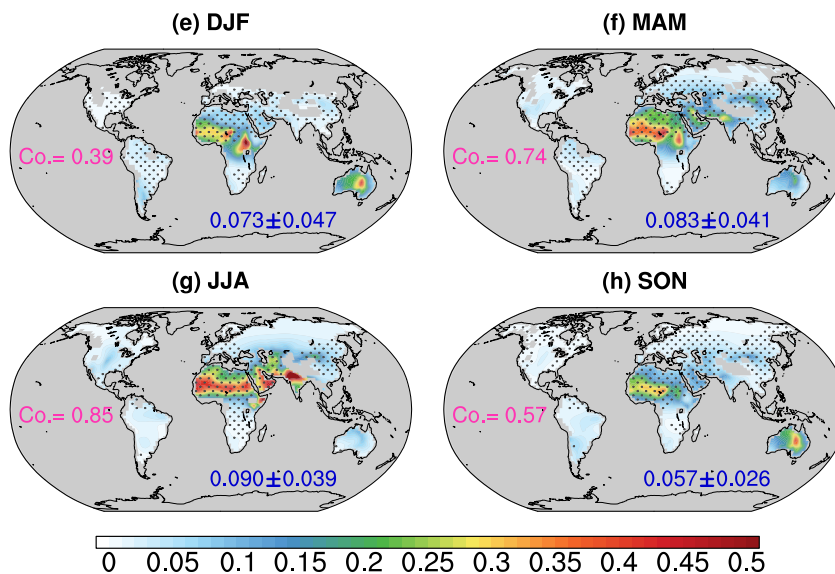
1198
Figure 1. Climatology (2004-2016) of Aqua and Terra combined DOD (i.e., MODIS
DOD; top panel) and multi-model mean of CMIP5 DOD (bottom) for four seasons. The
pattern correlation (centered; calculated after interpolating MODIS DOD to CMIP5 DOD
grids) between CMIP5 and MODIS DOD are shown in pink in the bottom panel. Blue
numbers denote global mean DOD over land. For CMIP5 model results, ± one standard
deviation among seven CMIP5 models is also shown. Black boxes in (b) denote nine
averaging regions (Table 2). Here we only added these boxes in (b) instead of every plot
to keep the figure clean. Note that CMIP5 multi-model mean is masked by MODIS DOD
for comparison. Dotted area in (e)-(h) shows where multi-model mean is greater than one
inter-model standard deviation.
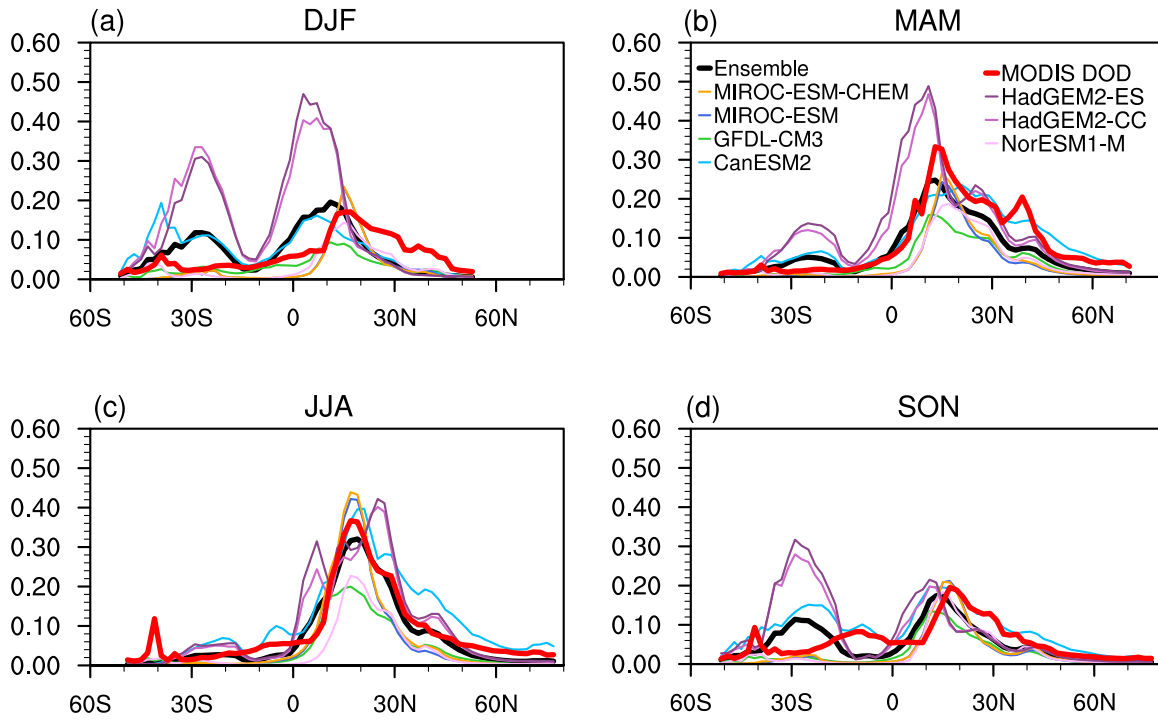
1209
1210 Figure 2. Zonal mean DOD from MODIS (thick red), CMIP5 multi-model mean (thick
1211 black), and each individual model (other colorful lines).
1212
1213
1214
1215
1216
1217
1218
1219
1220
1221
1222
1223
1224
1225
1226
1227
1228
1229
1230
1231
1232
1233
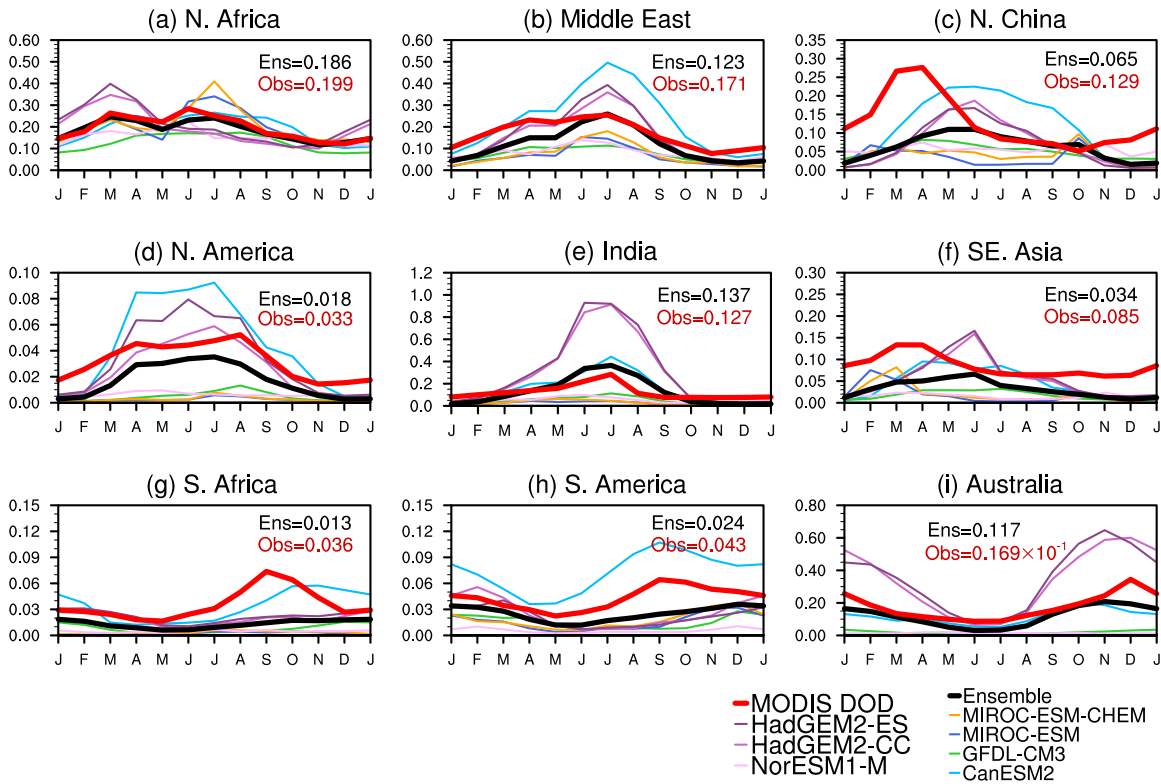
Figure 3. Seasonal cycle of DOD in nine regions (Table 2) averaged over 2004-2016. Thick red lines denote MODIS DOD, thick black lines denote CMIP5 multi-model mean, and other colorful lines denote individual model output. The annual means from MODIS DOD (Obs; red) and multi-model mean (Ens; black) are also listed in each panel. Note that in (i) MODIS DOD (red line) is scaled ten times to better display the season cycle.
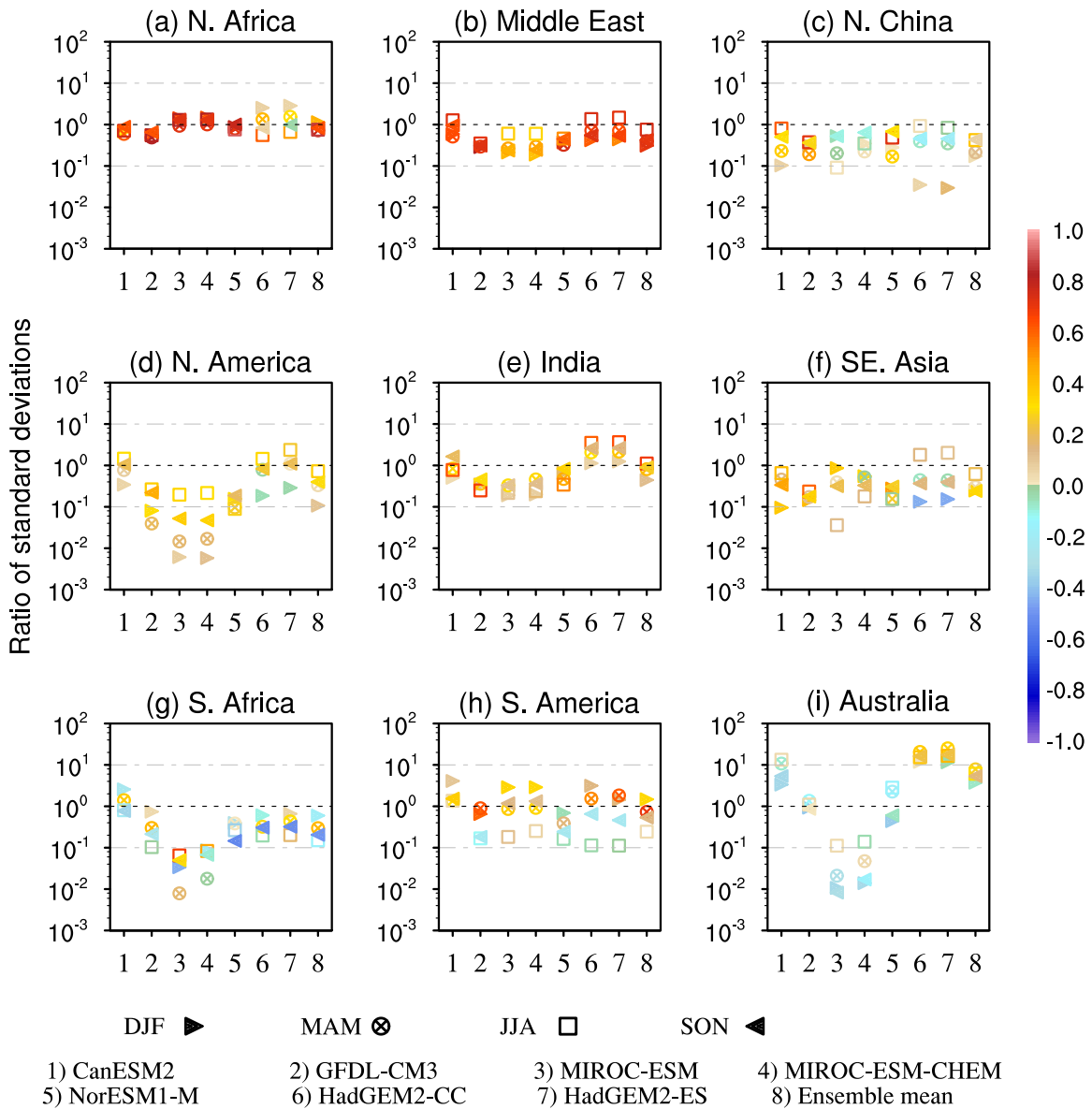
Figure 4. Spatial statistics comparing DOD from CMIP5 models with that from MODIS in nine regions. Label on the X-axis shows individual models (1-7) and multi-model mean (8). Y-axis shows the ratio of pattern standard deviations between model climatology (2004-2016) and that of MODIS, which reveals the relative amplitude of the simulated DOD versus satellite DOD. The color denotes pattern correlation (centered) between each model and MODIS DOD in each region.

DOD (CMIP5 vs. MODIS)

Figure 5. Correlations (color) between regional averaged time series from CMIP5 DOD and MODIS DOD from 2004 to 2016 for four seasons. Numbers in the X-axis denotes each model (1-7) and multi-model mean (8). Correlations significant at the 90% confidence level are marked by a star and significance at the 95% confidence level by two stars.
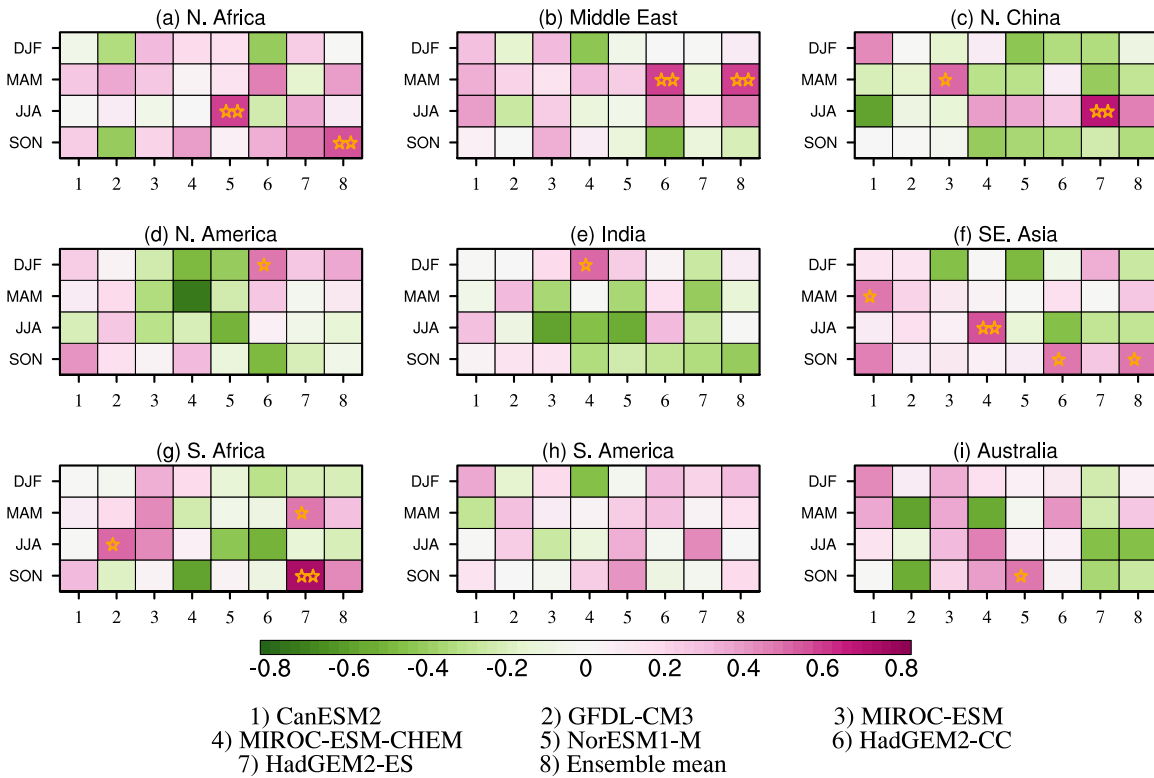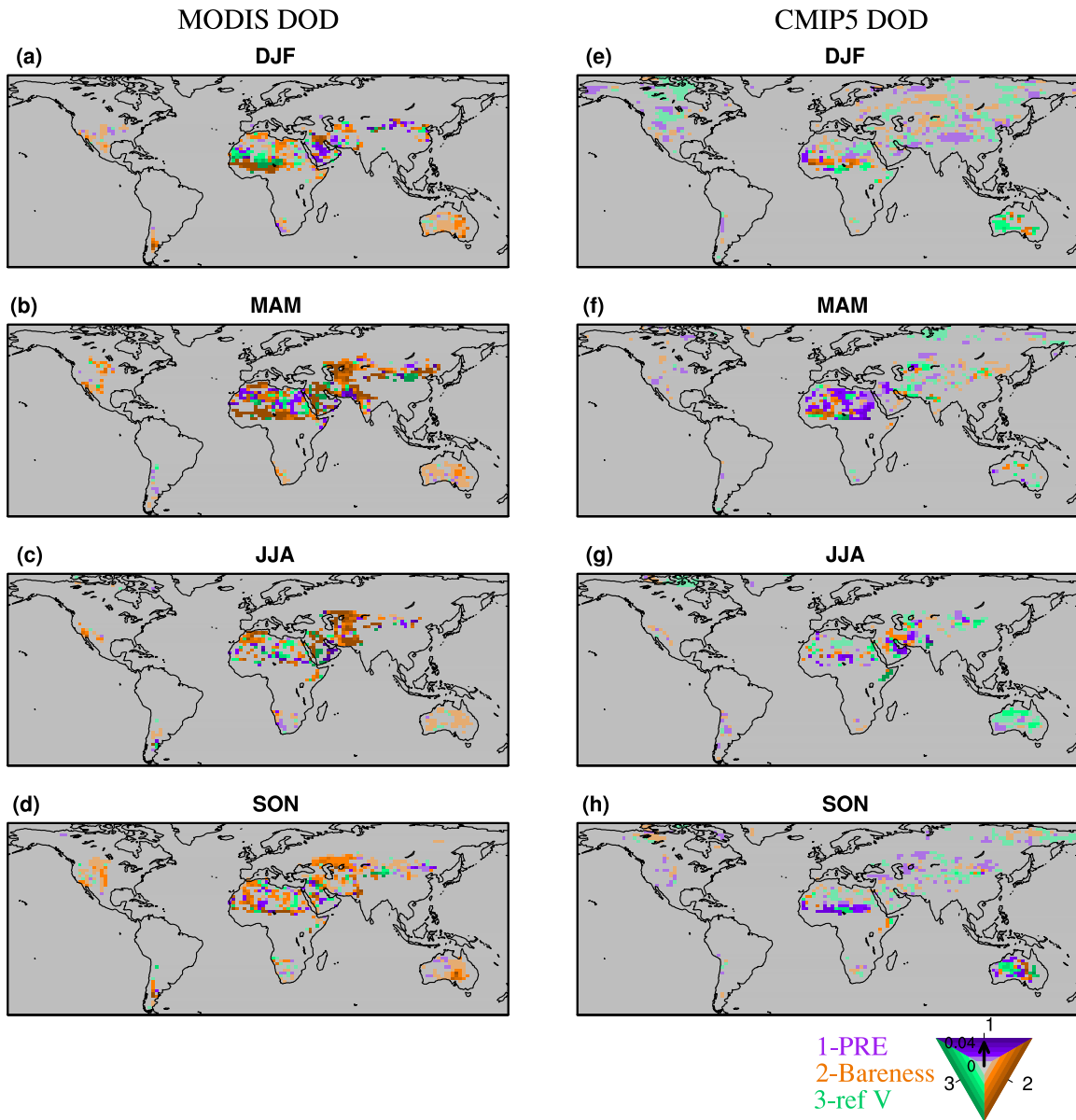
1275
1276
1277
1278
1279
1280
1281
1282
1283
1284
1285
1286
1287
1288
1289
1290
1291
1292
1293

1294
Figure 6. Regression coefficients calculated by regressing DOD in each season onto standardized precipitation (purple), bareness (orange), and surface wind speed (green) from 2004 to 2016. Coefficients obtained using MODIS DOD and observed controlling factors (interpolated to a 2° by 2.5° grid) and those using CMIP5 multi-model mean DOD and controlling factors are shown in the left and right columns, respectively. The color of the shading denotes the largest coefficient in absolute value among the three, while the saturation of the color shows the magnitude of the coefficient (from 0 to 0.04). Only regression coefficients significant at the 90% confidence level (Bootstrap test) are shown. Missing values are shaded in grey. To highlight coefficients near dust source regions, a mask of LAI ≤ 0.5 is applied.
1305
1306
1307

Changes of CMIP5 DOD (2051-2100 minus 1861-2005)

1308

1309 Figure 7. Projected changes of DOD in the late half of the 21st century (under the RCP
1310 8.5 scenario) from that in the historical level (1861-2005) by CMIP5 multi-model mean
1311 for four seasons. The percentage change of global mean (over land) DOD ± one inter-
1312 model standard deviation is shown at the bottom of each plot. Areas with sign agreement
1313 among the models reaches 71.4% (i.e., at least five out of seven models have the same
1314 sign as the multi-model mean) are dotted.

1315
1316
1317
1318
1319
1320
1321
1322
1323
1324
1325
1326
1327
1328
1329
1330
1331
1332
1333
1334
1335

Figure 8. Projected difference of (a)-(d) precipitation (mm day^{-1}), (e)-(h) bareness, and (i)-(l) 10 m wind (m s^{-1}) between the late half of the 21st century (2051-2100; RCP 8.5 scenario) and historical level (1861-2005) from multi-model mean of seven CMIP5 models. Areas with sign agreement among the models reaches 71.4% (i.e., at least five out of seven models have the same sign as the multi-model mean) are dotted.

Changes of regDOD (2051-2100 minus 1861-2005)
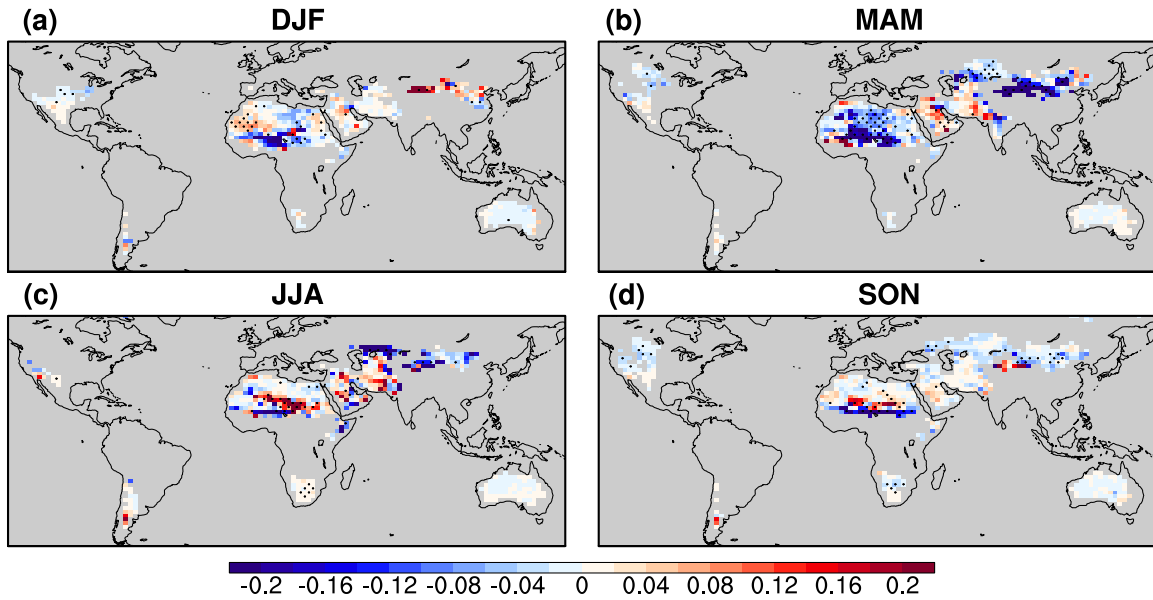
1360
1361 Figure 9. Projected change of DOD in the late half of the 21st century under the RCP 8.5
1362 scenario by the regression model. The results are calculated using the regression
1363 coefficients obtained from observations during 2004-2016 (see methodology) and
1364 projected changes of precipitation, bareness, and surface wind from seven CMIP5
1365 models. Dotted areas are regions with sign agreement among the regression projections
1366 (using output of each of the seven models) above 71.4% (i.e., at least five out of seven
1367 regression projections have the same sign as the multi-model mean projection). To
1368 highlight DOD variations near the source regions, a mask of LAI ≤ 0.5 (from present-day
1369 climatology) is applied.
1370
1371
1372
1373
1374
1375
1376
1377
1378
1379
1380
1381
1382
1383
1384
1385
1386
1387
1388

Changes of DOD (2051-2100 minus 1861-2005)
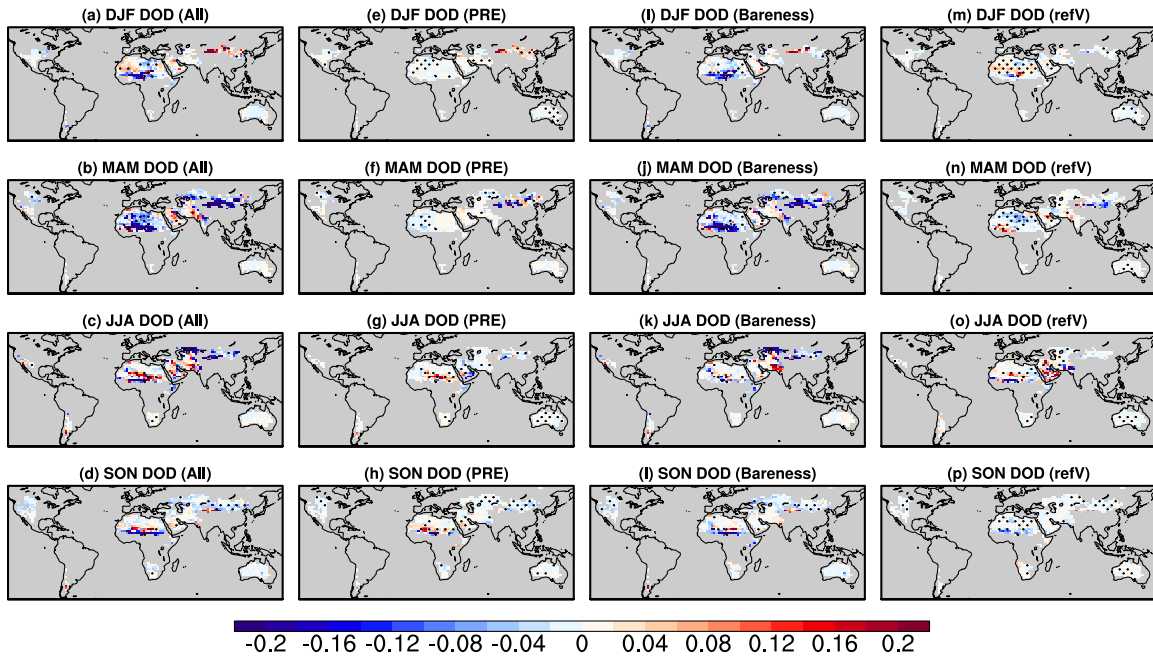
1391 Figure 10. (a)-(d) Projected change of DOD in the late half of the 21st century under the
1392 RCP 8.5 scenario by the regression model and output from seven CMIP5 models (same
1393 as Fig. 9), and contributions from each component, (e)-(h) precipitation, (j)-(i) bareness,
1394 and (m)-(p) surface wind speed. Dotted areas are regions with sign agreement among the
1395 projections above 71.4%. To highlight DOD variations near the source regions, a mask of
1396 LAI ≤ 0.5 (from present-day climatology) is applied.
1397